Estimation of Ionospheric Electrodynamic Parameters Using Ionospheric Conductance Deduced from Bremsstrahlung X-ray Image Data

B. -H. AHN
Cooperative Institute for Research in
Environmental Sciences
University of Colorado/NOAA
Boulder, CO 80309-0449

H. W. KROEHL
National Geophysical Data Center, NOAA
Boulder, CO 80309

Y. KAMIDE
Kyoto Sangyo University
Kyoto 603, Japan

and

D. J. GORNEY
Space Sciences Laboratory
The Aerospace Corporation
El Segundo, CA 90245

16 February 1989

Prepared for

SPACE DIVISION
AIR FORCE SYSTEMS COMMAND
Los Angeles Air Force Base
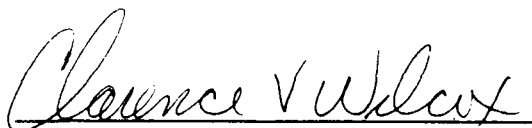P.O. Box 92960
Los Angeles, CA 90009-2960

DTIC
ELECTE
3 APR 1989
S
E
D

This report was submitted by The Aerospace Corporation, El Segundo, CA 90245, under Contract No. F04701-85-C-0086-P00019 with the Space Division, P.O. Box 92960, Los Angeles, CA 90009-2960. It was reviewed and approved for The Aerospace Corporation by H. R. Rugge, Director, Space Sciences Laboratory.
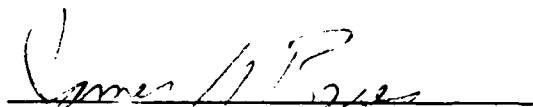
Lt Clarence V. Wilcox was the project officer for the Mission-Oriented Investigation and Experimentation (MOIE) Program.

This report has been reviewed by the Public Affairs Office (PAS) and is releasable to the National Technical Information Service (NTIS). At NTIS, it will be available to the general public, including foreign nationals.

This technical report has been reviewed and is approved for publication. Publication of this report does not constitute Air Force approval of the report's findings or conclusions. It is published only for the exchange and stimulation of ideas.

CLARENCE V. WILCOX, Lt, USAF
MOIE Project Officer
SD/CLTPC

JAMES A. BERES, Lt Col, USAF
Director, AFSTC West Coast Office
AFSTC/WCO

REPORT DOCUMENTATION PAGE

1a. REPORT SECURITY CLASSIFICATION Unclassified	1b. RESTRICTIVE MARKINGS

2a. SECURITY CLASSIFICATION AUTHORITY	3. DISTRIBUTION / AVAILABILITY OF REPORT Approved for public release; distribution unlimited.
2b. DECLASSIFICATION / DOWNGRADING SCHEDULE	

4. PERFORMING ORGANIZATION REPORT NUMBER(S) TR-0088(3940-06)-4	5. MONITORING ORGANIZATION REPORT NUMBER(S) SD-TR-89-08

6a. NAME OF PERFORMING ORGANIZATION The Aerospace Corporation Laboratory Operations	6b. OFFICE SYMBOL (If applicable)	7a. NAME OF MONITORING ORGANIZATION Space Division

6c. ADDRESS (City, State, and ZIP Code) El Segundo, CA 90245	7b. ADDRESS (City, State, and ZIP Code) Los Angeles Air Force Base Los Angeles, CA 90009-2960

8a. NAME OF FUNDING-SPONSORING ORGANIZATION	8b. OFFICE SYMBOL (If applicable)	9. PROCUREMENT INSTRUMENT IDENTIFICATION NUMBER F04701-85-C-0086-P00019

8c. ADDRESS (City, State, and ZIP Code)	10. SOURCE OF FUNDING NUMBERS			
	PROGRAM ELEMENT NO	PROJECT NO	TASK NO	WORK UNIT ACCESSION NO

11. TITLE (Include Security Classification)
Estimation of Ionospheric Electrodynamic Parameters Using Ionospheric Conductance Deduced from Bremsstrahlung X-Ray Image Data

12. PERSONAL AUTHOR(S) Ahn, B.-H. (University of Colorado), Kroehl, H.W., (National Geophysical Data Center), Kamide, Y. (Kyoto Sangyo University), and Gorney, D.J. (The Aerospace Corp.)

13a. TYPE OF REPORT	13b. TIME COVERED FROM _____ TO _____	14. DATE OF REPORT (Year, Month, Day) 1989 February 16	15. PAGE COUNT 58

16. SUPPLEMENTARY NOTATION

17. COSATI CODES			18. SUBJECT TERMS (Continue on reverse if necessary and identify by block number)
FIELD	GROUP	SUB-GROUP	Auroral zone Auroral electro Remote sensing

19. ABSTRACT (Continue on reverse if necessary and identify by block number)

Various ionospheric electrodynamic parameters for the period July 23-24, 1983, are calculated by using ground magnetic records from a total of 88 stations in the northern hemisphere. For this purpose, an 'instantaneous' conductance distribution deduced from the DMSP-F6 bremsstrahlung X-ray image data is utilized. Since the conductance distribution is, for the first time, completely independent of ground magnetic data, it is a unique opportunity to examine some of the inherent ambiguity in the magnetogram-inversion technique based on a statistically-derived conductance model. Several important conclusions of this study are: (1) The poleward portion of the westward electrojet in the morning sector is dominated by the electric field, while its equatorward portion is dominated by the ionospheric conductance. Although less definite, a reverse trend seems to pervade the eastward electrojet region in the dusk sector. (2) During a quiet or moderately disturbed period, the major electric potential pattern is roughly circumscribed by the auroral zone conductance belt with the subauroral

20. DISTRIBUTION / AVAILABILITY OF ABSTRACT ☑ UNCLASSIFIED/UNLIMITED ☐ SAME AS RPT ☐ DTIC USERS	21. ABSTRACT SECURITY CLASSIFICATION Unclassified
22a. NAME OF RESPONSIBLE INDIVIDUAL	22b. TELEPHONE (Include Area Code)	22c. OFFICE SYMBOL

DD FORM 1473, 84 MAR
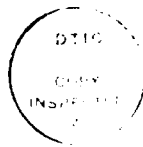83 APR edition may be used until exhausted
All other editions are obsolete

19. ABSTRACT (Continued)

zone being a substantially lower electric field region. (3) The global pattern of the equivalent current system resembles the electrical potential distribution. It may thus be possible to use the equivalent current system as a good approximation of the electric potential distribution in studying the magnetospheric convection pattern in the polar cap. '(4) The electric potential distribution consists generally of a smooth and well-defined two-cell convection pattern without any significantly localized structure. (5) A sunward convection flow is clearly identified over the polar cap region, during strongly northward IMF periods. The multi-cell nature of the convection pattern is still unclear. (6) During strongly northward IMF periods, significant currents and joule dissipation are observed in the polar cap region, indicating that the magnetosphere is far from its ground state. (7) The regions of intense joule heating are generally confined to relatively narrow belts along the auroral electrojets, with the major heating region in the westward electrojet region shifted poleward and the one in the eastward electrojet region shifted equatorward. The joule dissipation rate is relatively low in the local midnight sector. (8) The Region 2 upward current in the morning hemisphere is roughly collocated with the enhanced conductance region, while no corresponding conductance enhancement is found in the Region 1 upward current in the dusk sector. (9) The presently available statistical conductance models can be used, as a first approximation, to study global-scale polar ionospheric electrodynamics. However, the fact that the statistical models cannot simulate an instantaneous situation severely restricts their usefulness for studying the spatial and temporal variations of individual substorms.

PREFACE

Accession For	
NTIS GRA&I	☑
DTIC TAB	☐
Unannounced	☐
Justification	
By	
Distribution/	
Availability Codes	
Dist	Avail and/or Special
A-1	

CONTENTS

I. INTRODUCTION

During the International Magnetospheric Study (IMS, 1976-79) and the subsequent data analysis phase, it has been demonstrated (Fayermark, 1977; Kisabeth, 1979; Mishin et al., 1980; Kamide et al., 1981; Levitin et al., 1982; and Richmond and Kamide, 1988) that ground magnetometer data obtained from an improved network incorporated with the advanced computer algorithms are a powerful remote-sensing tool for estimating the global distribution of polar electrodynamic parameters. It has become possible to calculate ionospheric and field-aligned currents and electric potential and joule heating in the ionosphere. Furthermore, these "magnetogram-inversion" techniques have a great advantage in spatial coverage for a given instant, as well as high time resolution (say, 5 min.) over other more direct techniques, such as coherent and incoherent scatter radars and polar-orbiting satellites.

In order to compute the ionospheric electrodynamic parameters by using inversion schemes, an ionospheric conductance distribution must be provided as input. In the early phase of this effort to simulate the ionospheric conductance distribution, the auroral enhancement conductance model used by Kamide and Matsushita (1979) relied on a simple Gaussian form added to the 'background' solar UV origin conductance. Since then, several empirical conductance models (e.g., Vickrey et al., 1981; Wallis and Budzinski, 1981; Spiro et al., 1982; Ahn et al., 1983; Mishin et al., 1986; Fuller-Rowell and Evans, 1987; Hardy et al., 1987) have been devised primarily on the basis of long-term satellite measurements of particle precipitation and of ground magnetic perturbations. Employing such models, the magnetogram-inversion technique, introduced by Kamide et al. (1981), has been applied to IMS ground magnetometer data to study substorm dynamics (e.g., Kamide et al., 1982; Ahn et al., 1984). As pointed out by Kamide and Richmond (1982), however, some of the outputs of these inversion schemes (in particular, the electric potential and the joule heating rate) are highly sensitive to the choice of ionospheric conductance models. Furthermore, since

5

most of the conductance models devised so far are for average geomagnetic conditions, they may not be adequate in studying individual events, where enhanced conductivities are highly variable and localized. For all these reasons, the need for an accurate, instantaneous conductance distribution over the entire polar region has become acute.

Recently, Kamide et al. (1986) upgraded the so-called KRM scheme to incorporate an instantaneous conductance distribution that was estimated from Dynamics Explorer 1 (DE 1) auroral images combined with individual magnetograms. Although the scheme was more accurate than statistical conductance models in identifying the region of enhanced conductance, there are some inherent limitations to the method in estimating conductance from observed auroral emission intensity. Because of this shortcoming, Kamide et al. (1986) concentrated mostly on the ionospheric current pattern and the associated field-aligned current distributions during substorms, since both are less sensitive to the choice of conductance model than are electric fields and joule heating. On the other hand, instantaneous distributions of electron precipitation and ionospheric conductance have been produced using bremsstrahlung X-ray data from satellites (see Imhof et al., 1974, 1985, 1988; Mizera et al., 1978, 1984, 1985). Electron precipitation and conductance maps derived from X-ray data from the DMSP F2 and F6 satellites have been compared with results from other direct and remote sensing techniques (Rosenberg et al., 1987; Vondrak et al., 1988).

In this report, are presented the results of modeling efforts to estimate the distribution of ionospheric electrodynamic parameters for July 23-24, 1983, using ground magnetometer data from 88 northern hemisphere stations combined with the conductance distribution inferred from DMSP-F6 X-ray images. It is important to note that this is the first time that the magnetogram-inversion scheme is used with a realistic instantaneous (not average) conductance distribution. Thus, it is a great opportunity to examine the long-standing uncertainties in the outputs of the inversion technique that are caused by the use of statistically-determined conductance models during individual substorm events. In particular, an attempt

is made to differentiate, unambiguously, the relative importance of the
ionospheric conductance and electric field in the development of the
auroral electrojets. Furthermore, the joule heating rate and the cross-
polar-cap potential difference, both of which are important for thermo-
spheric and magnetospheric dynamics, are reevaluated based on the measured
conductance distribution.

II. DATA AND PROCEDURE

Magnetic records from a total of 88 stations in the northern hemisphere during the period July 23-24, 1983, are used in this study. The stations are listed in Table 1 and their distribution in corrected geomagnetic coordinates is plotted on an orthogonic projection in Fig. 1. A quiet day variation was removed to eliminate magnetic signatures of Sq-type current. In this case we used July 11, 1983, as the quiet day ($\Sigma kp = 8+$). The resulting values were then rotated into the corrected geomagnetic coordinate system of Gustafsson (1969) and labeled Xm and Ym, referring to the northward and eastward components, respectively, with 5-minute temporal resolution. We also constructed the auroral electrojet indices from the Xm values at stations between 55° and 75° in corrected geomagnetic latitude. Forty-four stations met the latitude criterion. Fig. 2 shows the AU(44) and AL(44) indices as well as data of the interplanetary magnetic field (IMF) during the two days. Since the DMSP satellite takes approximately 101 minutes to orbit the earth, the ionospheric conductance distribution can be obtained only about every 50 minutes, even if one assumes hemispheric conjugacy. The time required to image the entire polar region per orbit is about 17 minutes; thus, we averaged the four 5-minute values of the magnetic variations that were closest to each imaging interval.

In this study, it is assumed that the conductance has two components: one is a background conductance of solar ultraviolet origin, and the other is due to magnetospheric particle bombardment. We may call the former the quiet-time conductance and the latter the auroral-enhancement conductance. For the background conductance, we employed the model presented by Kamide and Matsushita (1979). For the auroral enhancement, we use the conductance distribution derived from DMSP-F6 bremsstrahlung X-ray data. The bremsstrahlung X-ray data consists of a measurement of the atmospheric backscattered X-ray energy spectrum above 1.5 keV within image pixels with horizontal dimension of about 100 km. The X-ray spectral measurements are used to infer the precipitating electron spectrum employing a

9

numerical optimization scheme (see, for example, Rosenberg et al., 1987).
Based on the estimated auroral electron spectra, the conductance is com-
puted from the steady-state ionization profiles derived from the altitude
profiles of energy deposition, following the method of Vickrey et al.
(1981). The X-ray technique provides a reasonable representation of the
important incident electron spectra parameters (see Rosenberg et al., 1987)
and makes it possible to estimate the ionospheric conductance (Vondrak et
al., 1988). Furthermore, a scanning X-ray detector like the one flown on
the DMSP-F6 satellite can image a large portion of two-dimensional electron
precipitation under both sunlit and dark conditions, while the particle
detector can provide data only along the satellite orbit. However, in
spite of the great advantages of an X-ray imager over other methods in
estimating the large-scale instantaneous ionospheric conductance distribu-
tion, there are several shortcomings due to the orbital characteristics of
the satellite and the limitations of the instrument. First, in its dawn-
dusk low-altitude polar orbits, the instrument's field of view is limited
to about 3000 km from one limb of the earth to the other, covering the
major portion of auroras only at the 'best viewing' situation. Second,
since the geomagnetic axis is tilted about 11° away from the rotational
axis and the inclination of the satellite is 99°, the satellite ground-
track footprint may miss the magnetic dawn-dusk meridian point by as much
as 20°, leaving a significant portion of the nightside or dayside aurora
out of the field of view. Third, it takes approximately 17 minutes for the
DMSP X-ray spectrometer to image the entire polar region, making it diffi-
cult to detect rapid variations in auroral intensity. Also, the consecu-
tive image of each hemisphere can be acquired only once per orbit, i.e.,
about every 101 minutes. However, on the assumption that there is a marked
auroral conjugacy between the northern and southern hemispheres (Akasofu,
1977, and references therein; Mizera et al., 1987), auroral images taken
over the southern polar region have also been utilized in this study. In
other words, we have a 17-minute image about every 50 minutes. Fourth, it
is not possible to apply this X-ray remote-sensing technique for precipi-
tating electrons at energies less than 1.5 keV. However, the exclusion of

the low-energy portion of the spectrum should not significantly affect our estimate of the Hall and Pedersen conductances since these particles do not penetrate deeply enough in altitude to contribute substantially to the E region conductivity (e.g., Strickland et al., 1983). Fifth, low signal-to-noise ratios also limit the X-ray technique to measurements of conductance values greater than 5 mhos for the Hall conductance and 2.5 mhos for the Pedersen conductance. Finally, to construct the global ionospheric conductance distribution caused by auroral particle precipitation, the spatial data gaps in the coverage of the instrument need to be filled in. The data gaps in the midnight portion of the auroral oval were interpolated by the data recorded in the dawn and dusk sectors, while the ones on the dayside were filled in by extrapolating (or stretching) the available data in the dawn and/or dusk sectors, recognizing that a minimum in conductance occurs near 1400 MLT (Hardy et al., 1987). In this way, maximum use of the measurements are used wherever they are available.

Once the ionospheric conductance distribution is specified, an electrostatic potential ϕ can be calculated via the equivalent current function of the observed ground magnetic perturbations. The numerical procedure is outlined in Kamide et al. (1982). The ionospheric current vectors are obtained from the curl-free electric field vector $\underline{E}$, i.e., $\underline{E} = -$ grad ϕ, and the conductance. The divergence of the ionospheric current yields the field-aligned current density. The Joule heating rate associated with the ionospheric current can also be obtained from these quantities.

In the following sections, we demonstrate the results of our numerical modeling by choosing four events, 0825-0840 UT, 1005-1020 UT, 1145-1200 UT and 2340-2355 UT, on July 23, 1983, as examples of the pre-expansion phase, the recovery phase, a quiet period, and the maximum phase of an intense substorm, respectively. The conductance distributions employed for these four events were based on the X-ray images obtained over the northern polar region.

11

III. 0825-0840 UT ON JULY 23, 1983

A substorm maximized at about 0920 UT on July 23, 1983, following an approximately seven-hour period of magnetic quiescence. This epoch is the period preceding the major expansion onset of an intense substorm. The equivalent current system in Fig. 3, which was obtained through the harmonic analysis technique by Kroehl and Richmond (1980), shows a well-defined two-cell pattern, plus a small-scale vortex on the dayside. The Hall conductance distribution estimated from the DMSP satellite X-ray image consists basically of an auroral oval-shaped enhancement. Except for the patch-like enhanced region in the late afternoon sector, the overall pattern is quite smooth along the nightside auroral belt during this period before the expansion onset of the substorm. The background conductance by the solar UV radiation dominates the dayside sector. As expected, the maximum value of the epoch is found at the noon sector. The numerical value shown at the bottom right-corner of the panel indicates the maximum value of the Hall conductance. Although it is not shown here, the Pedersen conductance distribution pattern has spatial characteristics quite similar to those of the Hall conductance, except for a reduction in the overall conductance value by a factor of roughly 2 in the auroral zone. Using the equivalent current function and conductance distributions as input, four ionospheric quantities, i.e., electric potential distribution, ionospheric current vectors, field-aligned current distribution, and joule heating rate, are obtained based on the magnetogram-inversion algorithm by Kamide et al. (1981). They are shown in Fig. 3.

The electric potential distribution pattern thus obtained consists of two well-defined vortices with the highest and lowest potential values located in the early morning and early afternoon sectors, respectively. The high potential vortex extends to the dayside, which is a signature of the positive IMF B_y component. The negative and positive numbers in the bottom right-corner identify these two extreme values. The cross-polar cap potential difference is simply the sum of the absolute value of the two

13

extremes; thus, it is 81 kV in this example. It is worth pointing out that in Fig. 2 the IMF B_y component was larger than 16 nT during the epoch. It is also worth mentioning that the major electric potential structure is restricted in latitude to the region north of ~67°, highlighting the relative importance of ionospheric conductance in the ionospheric current flowing equatorward of the region.

The ionospheric current distribution shown in Fig. 3 consists basically of the eastward and westward electrojets, which are of nearly equal intensities. Since the conductance distribution employed in this study is obtained completely independently of the magnetometer data, unlike the Ahn et al. (1983) technique, it is an opportunity to examine the relative locations of the electric field dominant and of the ionospheric conductance dominant in the auroral electrojet region. This question has been addressed by Kamide and Vickrey (1983), who suggested that some latitude/local time sectors of the electrojets are dominated by the electric field and others by the ionospheric conductance. The left-hand side of Fig. 4 shows the spatial relationship between the electric potential distribution and the region of the enhanced Hall conductance for the epoch shown in Fig. 3. Also shown is the relationship between the ionospheric current distribution and the enhanced regions of ionospheric conductance. The light and heavy shadings for the epoch of 0825-0840 UT represent the conductance of 4-8 mhos and >8 mhos, respectively. The strong current flows in the sunlit hemisphere seem to be associated with both the enhanced conductance distribution in the region originating from the solar UV radiation and the above-mentioned relatively strong electric field north of approximately 67° in latitude. It is noticeable that in the nightside auroral belt, only the equatorward half of the westward electrojet is embedded in the oval-shaped enhanced conductance zone. Furthermore, from the electric potential and conductance overlap plot in Fig. 4, it is quite clear that a significant contribution of the electric field to the westward electrojet in the post-midnight quadrant is only found north of approximately 67° in latitude. This characteristic of the westward electrojet in the early morning sector

has also been reported from radar measurements by Senior et al. (1982) and Foster (1987) and satellite particle measurements by Rostoker et al. (1985). Although this tendency is identifiable also in the midnight sector, we must remember that the ionospheric conductance around midnight for this particular epoch was interpolated using the available data from evening and morning hours.

It is worth pointing out that the electric potential pattern is similar to the equivalent current system in terms of their global features. This is an expected feature of the sunlit hemisphere, where the ionospheric conductance varies slowly with latitude and local time. On the other hand, the nightside also shows a resemblance between the two distribution patterns, indicating that slight auroral enhancements do not considerably influence the large-scale pattern.

In the field-aligned current distribution shown in Fig. 3, the Region 1 current in the morning sector is clearly identifiable, while it is slightly less prominent, yet still identifiable, in the dusk sector. With slightly reduced current density, the Region 2 current zones are also found in the dawn and dusk sectors.

As suggested by Kamide and Baumjohann (1985), however, the longitudinal uniformity of the field-aligned currents that is assumed in statistical studies of a large amount of polar-orbiting satellite data is not seen in this example, which in fact shows many local structures. It is interesting to notice that there are upward and downward currents poleward of the Region 1 currents in the dawn and dusk sectors, respectively. This sort of current system has been reported by Akasofu et al. (1980) from the IMS Alaska meridian chain magnetometer data, by Potemra et al. (1987), and by Bythrow et al. (1987) from the Viking satellite data. It may be the Region 0 Birkeland current suggested by Heikkila (1984).

The spatial relationship between the field-aligned current and the enhancement in the conductance is examined. The upward Region 2 current in the postmidnight quadrant coincides well with the conductance enhancement

15

in the same region. The upward Region 1 current in the dusk sector is also embedded in the enhanced conductance zone. However, the downward Region 2 current in the dusk sector is collocated with the enhanced conductance region. The strong upward current system in the cusp region without conductance enhancement seems to be associated with soft cusp region precipitation. It is also worth mentioning that the westward electrojet in the postmidnight sector flows across the Region 1 and Region 2 boundary, consistent with the radar measurement by Senior et al. (1982).

The distribution of joule heating shown in Fig. 3 clearly indicates that there are several major heating regions, including one in the westward electrojet in the early morning sector and one in the eastward electrojet in the dayside region. At the bottom left of the panel, the integrated joule heating rates from the pole to 80°, 70°, 60°, and 50° in latitude are listed in watts. The maximum heating is indicated at the bottom right of the panel in the unit of W/m^2. In this event, 59 mW/m^2 was registered, which is quite comparable with what the radar measurements by Vickrey et al. (1982) indicate. A close comparison of the heating patterns with the electrojet regions reveals that the high joule heating region in the post-midnight quadrant is located in the poleward half of the westward electro-jet, while the one in the afternoon sector is located in the equatorward portion of the eastward electrojet. Since the joule heating rate is the product of the Pedersen conductance and the electric field squared, $\Sigma p. E^2$, this type of spatial relation, particularly in the westward elec-trojet region, is a consequence of the fact that the poleward half of the westward electrojet in the morning sector is dominated by the electric field and the equatorward half by conductance enhancement. Although the spatial relationship between the two quantities for the eastward electrojet is not as prominent as in the case of the westward electrojet, the slight equatorward shift of the enhanced joule heating region with respect to the center of the eastward electrojet seems to suggest that conductance is more important than electric field in the poleward portion of the eastward elec-trojet in the afternoon sector. Robinson et al. (1982, 1985) also sug-

gested the different roles of conductance and electric field in the east-
ward and westward electrojet regions.

IV. 1005-1020 UT ON JULY 23, 1983

This epoch is just after the maximum phase of the substorm. The equivalent current system in Fig. 4 again shows a well-defined two-cell pattern. In particular, an enhancement and the equatorward expansion of the counterclockwise current vortex in the afternoon-evening sector is noticeable. Unfortunately, however, there is some degree of uncertainty in the poleward portion of the vortex, because it is coincident with the Arctic Ocean, where no observed data were available. Thus, one should be cautious in interpreting the physics in the region.

The Hall conductance distribution shows a significant enhancement along the entire auroral belt with regions of structured precipitation. There is also an indication of an equatorward shift of the overall pattern, particularly in the midnight sector. However, since the conductance data around the midnight sector have been estimated through interpolation due to the data gap in the region, it is impossible to determine the exact latitudinal shift. In the dawn and dusk sectors, where conductance measurements were available, both the poleward and equatorward expansions of the belt are noticeable.

The electric potential distribution in Fig. 5 consists of a typical two-cell pattern and shows a significant overall enhancement along with an equatorward expansion, compared to the corresponding pattern in Fig. 3. The cross-polar cap potential difference is 109 kV, an increase of 28 kV over the previous epoch. As in the previous event, the IMF By positive signature is clearly seen on the dayside in this example. In contrast to the previous case, the location of the nightside potential vortex is now moved towards midnight, compared with the equivalent current pattern. As noticed in the previous example, the enhanced conductance region is generally located equatorward of the electric field dominant region except for patch-like enhancements embedded in the negative potential cell in the dusk sector. Furthermore, if one takes into account the fact that the entire

19

polar region during the summer season is moderately conducting, the similarity between the electric potential and equivalent current distributions in their large-scale patterns is not surprising. There is a narrow region of exception along the equatorward half of the westward electrojet in the postmidnight sector. However, it does not seem to affect the global distribution pattern to any considerable degree.

The characteristics of the ionospheric current distribution are basically similar to those of the previous epoch. In particular, the current pattern around the local noon sector, flowing eastward at higher latitudes and westward at lower latitudes, which reflects the IMF By positive situation, has not changed significantly. Actually, the unusually large positive IMF By component, greater than 20 nT, has persisted until about 1000 UT (see Fig. 2). The westward electrojet in the prenoon to midnight sector through the dawn shows a moderate enhancement while shifting equatorward several degrees. On the other hand, the eastward electrojet accompanied by a very intense westward current flow at higher latitudes shows a strong enhancement without any noticeable latitudinal shift. The spatial relationship between the ionospheric current and the ionospheric conductance in the electrojet regions reveals that the equatorward half of the westward electrojet in the morning sector is dominated by the conductance, while its poleward half is dominated by the electric field enhancement. While not as obvious as in the westward electrojet region, an opposite trend prevails in the eastward electrojet region; namely, the conductance enhancement seems to be more important than the electric field increase in the poleward portion. Furthermore, each electrojet has its own characteristics for its poleward and equatorward portions; the eastward electrojet, as a whole, seems to be generally dominated by the electric field, whereas the westward electrojet is dominated by conductance enhancement. It is quite clear in this particular example. Note that, in spite of the small-scale patch-like conductance enhancement, the overall conductance in the dusk sector is slightly less than or, at most, comparable to that in the dawn sector, while the ionospheric current intensity of the eastward elec-

20

trojet region in the dusk sector is stronger than that of the westward electrojet region. By comparing the Chatanika radar measurements of the electric field with the simultaneous College ground magnetic perturbations, Ahn et al. (1983) showed that there exist different empirical relationships between the electric field and the horizontal magnetic perturbations for positive and negative magnetic variations, with a stronger electric field being associated with the eastward electrojet region than with the westward electrojet region for the same magnitude of magnetic variations. Our results confirm those characteristics.

The field-aligned current distribution pattern in Fig. 5 shows the signature of Region 1 and Region 2 current systems. The maximum current densities of the Region 1 current found in the forenoon and late afternoon sectors are 2.6 and 2.4 μA/m2, respectively, where the negative value represents upward current flow. It is in good agreement with the statistical study by Iijima and Potemra (1976) in terms of the location and magnitude of the maximum current. A pair of weak current systems poleward of the Region 1 current, suggested by Heikkila (1984) as the Region 0 current system, are also seen in this event. The Region 2 upward current in the morning hemisphere is roughly collocated with the enhanced conductance region. Although the region of the strong upward Region 1 current in the afternoon sector is embedded in the moderately enhanced conductance zone due to the solar UV radiation, there seems to be no corresponding conductance enhancement due to auroral precipitation, suggesting the softness of the precipitating electron spectra in the region.

The Joule heating pattern of this epoch is basically the same as that of the previous epoch, with two major heating regions collocated with the two electrojet systems. It is worthwhile mentioning, however, that there is no significant heat production in the local midnight sector. One can also notice a similar tendency in the previous epoch, although the low heat production region is shifted toward the premidnight quadrant. Banks (1977) described such a heating pattern as 'horseshoe shaped'. A similar pattern has been reported by Vickrey et al. (1982) and Kamide et al. (1986).

V.   1145-1200 UT ON JULY 23, 1983

Magnetic activity during this period was as low as 142 nT in terms of the AE(44) index. As expected, no appreciable magnetic variation is found at auroral latitudes: See the equivalent current vector plot in Fig. 6, which is constructed simply by rotating the horizontal magnetic perturbation vector 90° clockwise. It is interesting to note, however, that very strong magnetic perturbations were observed over the polar cap and dayside cusp regions. During this period the IMF was directed northward and the B_z component registered an extremely high value, ~20 nT: See Fig. 2. Thus, it seems that the high-latitude polar region is no longer quiet during a period of such a large positive IMF B_z component. By examining electron precipitation patterns in the highest latitude region, Meng and Makita (1987) concluded that a truly quiet magnetospheric condition is established during periods of very weak IMF.

Six polar-plot diagrams for this period are shown In Fig. 7. As mentioned earlier, the similarity between the equivalent current system and the electric potential pattern is quite understandable from the fact that the major ionospheric current flows are confined to the relatively uniform solar conductance region. Furthermore, the weakly enhanced conductance regions at auroral latitudes, which are clearly seen in the Hall conductance distribution plot in Fig. 7, do not seem to affect significantly the electric potential pattern in the region, since no appreciable ionospheric current is associated with it.

The potential distribution pattern in Fig. 7 has a unique feature, completely different from the two previous examples. Although it is skewed slightly toward the early afternoon sector, a sunward convection flow over the polar cap region is perfectly clear. Furthermore, a 'reversed' two-cell convection pattern is identifiable north of about 80° in latitude, with the negative cell in the prenoon quadrant and the positive one centered in the dusk sector less prominent and stretched toward the midnight sector. How-

23

ever, it should be mentioned that there seems to be a significant amount of uncertainty in the dusk sector cell due to the dearth of magnetic stations in the premidnight quadrant north of 70° in latitude; see the station distribution in Fig. 6. Such a sunward convection flow during the northward IMF period has been reported from analyses of ground magnetic data (Friis-Christensen and Wilhjelm, 1975; Maezawa, 1976; Horwitz and Akasofu, 1979; Rezhenov, 1981; Ahn et al., 1987) and satellite measurements (Burke et al., 1979; Reiff, 1982; Zanetti et al., 1984; Heelis et al., 1986). Although it is premature to draw any conclusion about the multicell nature of the convection pattern during this epoch, the overall form seems to consist of three cells: a negative potential cell in the prenoon quadrant with some extension toward the afternoon sector; a positive cell extending from early afternoon to the midnight sector through the dusk; and another negative cell in the premidnight quadrant with its center located at 70° in latitude. Under the boundary condition that the electric potential value of the pole is 0 kV, the maximum values of the three cells are -46, 20, and -25 kV, respectively. Recently, from the analysis of DE 2 electric field measurements, Heppner and Maynard (1987) have proposed an interesting electric field model for strongly northward IMF periods. According to them, the sunward convection flow is simply a distorted regular two-cell configuration rather than a multicelled potential pattern. It is interesting to compare the electric potential pattern in Fig. 7 with the distorted model during a strongly positive B_z period studied by Heppner and Maynard (their Fig. 12). If one assumes that the two negative potential cells in Fig. 7, one centered in the prenoon and the other in the premidnight sector, are in fact connected, the two potential distribution patterns are quite similar to each other in terms of the general configuration and the orientation of convection flows. Such an assumption seems to be supported by the ionospheric current distribution pattern in Fig. 7. Notice the relatively strong and steady current flow from midnight to noon through dusk, roughly along the latitude circle of 75°. Thus, we may conclude that the electric potential distribution consists of a distorted two-cell pattern even during such a strongly positive IMF period. However, because of the data gap,

24

there still remains some uncertainty about the high-latitude premidnight quadrant. From an analysis of ground magnetic data, Ahn et al. (1987) reported that the multicell convection pattern is seldom observed during a prolonged northward IMF period. The cross-polar cap potential difference is obtained simply by adding the two extreme potential values, the positive one usually located in the dawn and the negative one in the dusk sector. The potential difference thus obtained is 66 kV. However, it should be mentioned that the numerical value of the potential difference itself does not tell whether it is associated with a normal convection flow or a reversed one. Although the major potential structure is confined within the higher latitude region, the cross-polar cap potential difference is significantly large, indicating that a considerable amount of energy is flowing into the magnetosphere during such a strongly northward IMF period, as suggested by Iijima et al. (1984) and Meng and Makita (1987).

The ionospheric current distribution in Fig. 6 does not show much systematic flow pattern. A significant one is found only in the dusk hemisphere along the latitude circle of about 75°. The relatively strong current flows in the polar cap region are convincing evidence that strong activity is occurring in the high-latitude region during the strongly positive IMF B_z period. On the other hand, at auroral latitudes, only a weak eastward electrojet is noticeable in the dusk hemisphere. Since the distribution of magnetic observatories is dense enough in the morning hemisphere, the absence of an appreciable westward electrojet seems to be a realistic situation. This is one reason why the standard AE(12) index, which registered 99 nT during this period, cannot accurately monitor the global magnetic activity during such a situation.

The field-aligned current distribution also shows quite unusual characteristics with two pairs of oppositely flowing current systems located in the highest latitude region. The pair in the dayside sector, flowing upward in the prenoon quadrant and downward in the postnoon quadrant, looks like the NBZ Birkeland current system proposed by Iijima et al. (1984) during a northward IMF period. The maximum current densities of the upward

and downward current regions are 2.9 and 2.0 μA/m2, respectively. These
are large and quite comparable with those of the Region 1 currents in the
two previous examples. As can be seen from the Hall conductance distribu-
tion in the same figure, however, there is no structured conductance en-
hancement in the region, thus suggesting that soft electron precipitation
is the current carrier. In the night hemisphere, there is another pair of
field-aligned currents which flow in the directions opposite to those in
the dayside hemisphere. Unfortunately, we cannot be absolutely certain
that these currents are authentic, since the upward current region in the
premidnight quadrant is collocated with the data gap mentioned earlier.
Besides the current system in the highest latitude region, the Region 1 and
2 current systems in the dusk hemisphere are identifiable. Although such a
signature in the dawn hemisphere is not prominent, a downward current flow
confined mainly to the prenoon quadrant may be Region 1 current. Less
prominent than the downward current flow, a hint of upward current flow is
also noticeable in the same quadrant.

The joule heating rate shown in Fig. 7 indicates a strong dissipation
in the polar cap region. Although the major heating region is confined
within a relatively narrow region, poleward of 75° in latitude, the global-
ly integrated heating rate is as large as 1.2 x 1011 watts, suggesting that
a considerable amount of energy is flowing into the magnetosphere during
such a strongly northward IMF period. Furthermore, the amount of energy
being released as joule dissipation is comparable to the solar wind energy
coupling function ~10^{11} watts, during which, according to Akasofu (1983),
the joule dissipation in the ionosphere and the brightness of the aurora
become appreciable. Thus, as suggested by Meng and Makita (1987), the
magnetosphere seems to be far from its ground state during such a strongly
northward IMF period.

It is interesting to note that the Hall conductance distribution pat-
tern in Fig. 7 shows a well-defined conductance-enhanced zone along the
auroral latitude, without any appreciable auroral electrojet (AE). Thus it
seems that an enhancement of conductance even in the nightside auroral zone

26

does not necessarily accompany a strong ionospheric current. In other words, the enhancements of the electric field and ionospheric conductance do not always occur concurrently. A comparison of the conductance distributions of the epoch at 0825-0840 UT in Fig. 3 with that of this event sheds some light on this matter. Except for several patch-like enhancements in the former event, the two patterns are comparable in terms of the magnitude and geographic locality of the enhanced conductance distribution. However, the magnetic activity in terms of the AE index was recorded at 490 nT for the former epoch and 140 nT for the latter epoch. Thus, to derive such a relatively intense auroral electrojet in the former epoch, a strong electric field is required, which is evident from the comparison of the electric potential distributions of the two events. Since the former epoch is during a pre-expansion phase and the latter during a late recovery phase, or a quiet period, it further seems that the electric field enhancement is more important than the conductance increase during the early phase of a substorm; or perhaps ionospheric conductance enhancement is a more permanent feature at auroral latitudes than is electric field enhancement.

Soon after the first substorm on July 23 subsided, both the AU and
|AL| indices gradually increased again. A period of almost continuous sub-
storm activity persisted until 1000 UT on the 24th. The example chosen
here is shortly after the maximum phase of a substorm that occurred at
about 2325 UT on July 23. From the Hall conductance distribution in Fig.
8, one can see clearly that, besides an overall enhancement, there is a
surge-like enhancement in the midnight sector, indicating that this is
during the maximum phase of a substorm or shortly thereafter. Although it
is not shown here, the Pedersen conductance distribution shows a rather
moderate enhancement in the morning and midnight sectors. A comparison
between the two patterns reveals that the electron spectrum in the morning
sector is harder than that in the evening sector, with the Hall-to-Pedersen
conductance ratio being approximately 3 at the auroral latitude in the
midnight and morning sectors. The equivalent current system and the elec-
tric potential distribution pattern are shown in Fig. 8. As pointed out
for the previous three events, the similarity between the two patterns is
also readily evident.

A comparison of the potential distribution pattern of this epoch with
that at 0825-0840 UT in Fig. 3 yields several interesting results. First,
during both epochs the cross-polar cap potential difference was 81 kV. But
the magnetic activities of the two epochs in terms of the AE(44) index were
562 nT and 1062 nT at 0825-0840 UT and 2340-2355 UT, respectively. Thus
the intensification of the auroral electrojets in the latter epoch seems to
be associated more with a global enhancement of the ionospheric conductance
than with the electric field increase. This tendency for there to be an
increase in the ionospheric current density before the substorm onset is
primarily due to the electric field enhancement. The fact that relative
predominance of the ionospheric conductance starts only after substorm
onset was also reported by Kamide and Baumjohann (1985). Second, since the
two events are not consecutive, it may be difficult to make a direct com-

parison, particularly of the morphological evolution. Bearing in mind this limitation, we examined separately the change in each potential cell. With the absolute value of the negative cell centered in the late afternoon sector, the value relative to the pole (which is assigned 0 volt as a boundary condition) increased from 32 to 47 kV, while the positive cell showed a decrease of 15 kV. It seems partly due to the change of IMF B_y component from positive during the earlier epoch to negative during the later epoch (Friis-Christensen et al., 1985). With the overall magnetic activity increase in terms of the AE index, however, there is no particular reason to expect the negative potential cell in the afternoon sector to become enhanced while the positive one in the morning sector is subsiding. Therefore, the intensification of the conductance during the maximum phase of a substorm seems to be partly responsible for the reduction of the electric field in the midnight-morning sectors. (Notice that the equatorward edge of the positive cell is embedded in the enhanced conductance zone.) Third, while maintaining the basic two-cell structure, the whole potential pattern has expanded significantly equatorward. Fourth, as mentioned above, one can further notice that an interesting change in the potential pattern over the dayside sector has occurred, clearly reflecting the fact that the two epochs were under different IMF B_y conditions.

The ionospheric current distribution shown in Fig. 8 is also compared with that at 0825-0840 UT in Fig. 3. With an overall intensification of ionospheric current, the 4° equatorward shift of the electrojets is clearly visible. In particular, the shift of the eastward electrojet in the post-noon sector is more prominent than that of the westward electrojet in the postmidnight sector. Analyzing ground magnetograms, Rostoker and Phan (1986) obtained a similar result. During the maximum phase of a substorm, it has been reported that the westward electrojet intrudes far into the evening sector along the poleward boundary of the eastward electrojet. Although there is a hint of such an intrusion in this epoch, it is not as clear as in the studies by Ahn et al. (1984, 1986). Since this epoch is about 15 minutes after the maximum phase, as suggested by Kamide (1982),

the intruded portion of the westward electrojet seems to have started its retreat toward the morning sector. The spatial relationship between the ionospheric current and the conductance enhancement is again of some interest. On the right-hand side of Fig. 4 overlapping plots are shown, with the light and heavy shaded areas representing the enhanced Hall conductance regions of 16 - 24 mhos and >24 mhos, respectively. As pointed out earlier, the equatorward portion of the westward electrojet in the morning sector is embedded in an enhanced conductance zone, while its poleward portion seems to be located in a strong electric field region. In the overlapping plot showing the spatial relationship between the electric potential distribution and the conductance enhancement in the same figure, the electric field dominant region in the morning sector is identified as the region with the relatively dense potential contour distribution located poleward of the enhanced conductance zone. However, a somewhat different situation is found in the midnight sector, where an enhanced conductance zone is collocated with the westward electrojet. Furthermore, there is an enhanced conductance zone with no significant accompanying ionospheric current, equatorward of the westward electrojet in the postmidnight quadrant, suggesting that, even in the nightside auroral latitude, an enhancement of conductance does not necessarily accompany an enhanced ionospheric current. On the other hand, except for a patch-like enhancement in the dusk sector, most of the eastward electrojet is located in the region of enhanced conductance of solar UV origin. Thus, as mentioned earlier, the eastward electrojet seems to be generally dominated by the electric field.

The field-aligned current distribution in Fig. 8 also shows well-defined Region 1 and Region 2 current systems both in the dawn and dusk hemispheres, except for the downward Region 2 current being confined within the postnoon quadrant. As mentioned earlier, only the upward Region 2 current in the morning sector is reasonably well matched with the enhanced conductance zone, indicating that the electron spectrum is hard enough to produce a significant conductance enhancement in the region. On the other hand, there are relatively strong field-aligned current flows in the day-

31

side sector compared to the midnight auroral zone. Such a tendency has also been found in all three previous epochs. However, no significant field-aligned current is found in the polar cap region.

The isocontours of the joule heating rate in Fig. 8 show that the major heat production regions roughly delineate the auroral electrojets, suggesting a close association between the two quantities. However, a closer look reveals that the major heating region in the morning sector is located along the poleward portion of the westward electrojet, thus supporting the earlier conclusion that the electric field is more important than the conductance in the poleward portion of the westward electrojet and that the opposite trend prevails in its equatorward portion. On the other hand, although the evidence is less certain, the tendency seems to be reversed in the eastward electrojet region. Note that the maximum joule heating region in the postnoon sector is shifted slightly equatorward of the center of the eastward electrojet. As expected, however, the local midnight sector, where the conductance enhancement seems to be more important than the electric field, does not show any significant joule dissipation. The relative quiescence of the polar cap region in terms of the joule heating also deserves mention. Comparing the integrated heating rates from 80° to the pole for this event and that at 1145-1200 UT in Fig. 7, one can notice that the latter is larger than the former by a factor of 3.4. In contrast, the globally integrated heating rate from the pole to 50° in latitude is larger by a factor of 2 in this epoch than the one depicted in Fig. 7. Therefore, it is again confirmed that the polar cap region is relatively quiet during a disturbed period, while it becomes the most dynamic region of the entire polar area during a strongly northward IMF period. Furthermore, it is worthwhile to point out that the globally integrated joule heating rate during such a strongly northward IMF period can be as large as 50% of that during a typically disturbed period.

VII. COMPARISON BETWEEN THE STATISTICAL AND 'INSTANTANEOUS' CONDUCTANCE MODELS

This study provides a unique opportunity to evaluate how closely the statistically constructed conductance models can simulate the real situation, which can be known well enough through satellite X-ray image data. Because many studies using magnetogram-inversion techniques have relied on statistical conductance models, it is also important to examine the degree of uncertainty in the outputs caused by adopting an unrealistic conductance distribution. For the purpose of comparison with the 'realistic' conductance distribution based on the X-ray image data, the conductance distribution during 2340-2355 UT on July 23, 1983, is simulated based on the conductance models by Spiro et al. (1982) and by Ahn et al. (1983). With the ground magnetic data and the simulated conductance distribution as input, various ionospheric parameters are obtained through the same procedure as employed in this study. From the output parameters, the electric potential and the joule heating distributions, which were reported to be most sensitive to the choice of the ionospheric conductance model (c.f. Kamide and Richmond, 1982), are compared with their counterparts based on the 'realistic' conductance distribution shown in Fig. 8. The left-hand side of Fig. 9 shows the Hall conductance distribution for the epoch simulated from the model by Ahn et al. (1983), which utilizes ground magnetic perturbation data, and the corresponding electric potential and joule heating distributions as outputs. The right-hand side shows the distributions of the same quantities based on the model detailed in Spiro et al. (1982), which is parameterized by the AE index.

Several interesting points emerge from the comparison of the three Hall conductance distributions. First, the maximum values of the two statistical conductance distributions, listed in the bottom right-corner of each panel in the unit of mho, are slightly larger than that of the one observed from X-ray image data. They are 26, 30, and 34 mhos for the X-ray image-based, Ahn et al. and Spiro et al. conductance distributions, respec-

tively. Thus, these statistical models seem to overestimate the peak conductance. This possibility has been already discussed by Vickrey et al. (1981) and Robinson et al. (1987). Second, although it is to be expected, the enhanced regions of conductance in the statistical models are not generally well matched with those of the X-ray image-based conductance distribution. As far as this example is concerned, the major enhanced conductance belt both in the X-ray image-based and Ahn et al. conductance distribution is located in the midnight-morning sector, while the one in the Spiro et al. model is found in the midnight-dusk sector. On the other hand, there is an additional enhanced conductance belt in the noon-dusk sector of the Ahn et al. model, which is absent from the other two distributions. Third, the enhanced conductance belts along the auroral zone for the statistical models are narrower and relatively smoother than that of the observed one. The smoothness seems to be a consequence of the statistical processing of data. Fourth, the conductance values below 60° in latitude of both statistical models are significantly lower than that of the observed model. Thus, the statistical models seem to underestimate, systematically, the conductance in the subauroral zone in this case. All these characteristics have important consequences, particularly for the distributions of the electric potential and the Joule heating rate.

In spite of the apparent differences among the conductance distribution patterns, the three electric potential distribution patterns show a marked similarity in their overall global patterns, in that all three diagrams have well-defined two-cell patterns. The similarity seems to result mainly from the fact that the period under study was during a summer season and thus a significant portion of the polar region is influenced by the sunlit conductances. In particular, one can see a better resemblance in the dayside hemisphere, including the IMF B_y negative signature of the convection pattern. However, a detailed comparison of the potential patterns reveals significant differences, particularly in the nightside auroral region. First of all, the cross-polar-cap potential differences, one of the most important input parameters for magnetospheric convection

34

modeling studies, are 81, 85, and 64 kV for the X-ray image-based, Ahn et al. and Spiro et al. conductance distributions, respectively. Since the Spiro et al. model generally overestimates the conductance value, the potential difference based on it should be less than that based on the observed conductance distribution. However, the potential distribution based on the Ahn et al. model is larger than what is expected and even larger than the observed situation. This large value can be understood if one remembers that, although the maximum value of the conductance distribution is larger than that of the observed case, the enhanced conductance zone in the Ahn et al. model is considerably narrower than that of the observed situation, thus enlarging the potential difference. Actually, the parameter determining the width of the Gaussian type enhanced conductance belt in the Ahn et al. model was chosen empirically and needs to be tested vigorously with a more direct measurement. Second, the most prominent difference is found in the subauroral zone of the night hemisphere below 60°, where a significant electric potential structure exists in both patterns based on the statistical models, while no such signature is evident in the observed situation. In particular, notice a prominent vortex structure below 60° in the premidnight sector of the potential distribution based on the Spiro et al. model. Although less prominent, a similar pattern is also noticeable in the distribution based on the Ahn et al. model. Such relatively strong electric fields in the subauroral zone have been reported quite often in recent magnetogram-inversion studies, employing one of the statistical conductance models, and have been interpreted as being a result of the unrealistic assumption that magnetic field lines in the region are essentially vertical (Kamide and Baumjohann, 1985). However, it actually has more to do with the unrealistically low conductance distribution in the statistical conductance models than with the unrealistic assumption of verticalness. Third, due to the overestimation of the conductance in the nightside auroral latitude in the statistical conductance models, the electric field strength based on these models is generally underestimated in that region. Such a trend is clearly seen in the potential distribution pattern based on the Spiro et al. model, where the weak electric field

region in the nightside hemisphere roughly coincides with the enhanced conductance region, thus leaving the auroral latitude with the weakest electric field region of the nightside hemisphere. On the other hand, the Ahn et al. model is slightly closer to the observed case in Fig. 8. As mentioned above, however, it also includes a considerably enhanced electric field region of the subauroral latitude in the nightside hemisphere.

The Joule heating rates based on the three conductance distributions for the epoch of 2340-2355 UT on July 23, 1983, are also compared. As expected from the electric potential distribution patterns, the global features of the three distributions are quite similar, with the two major heating regions being roughly collocated with the auroral electrojets. Furthermore, the globally integrated heating rates from the pole to 50° in latitude for the X-ray image-based, Ahn et al., and Spiro et al. conductance distributions are 2.2×10^{11}, 2.0×10^{11}, and 1.9×10^{11} watts, respectively, thus suggesting that the global quantity is not very sensitive to the choice of conductance model. The slight underestimation of the global Joule heating rate in the statistical cases is easily explained when one recalls that the ionospheric conductance value along the auroral latitude in the statistical models is generally overestimated. However, a more detailed comparison between the Joule heating patterns based on the statistical conductance models with those based on the observed case provides another insight into the consequences of assuming an unrealistic conductance distribution. The maximum heating rate in the observed case is about 51 mW/m2 while the other two cases registered 26 mW/m2 for the Ahn et al. model and 30 mW/m2 for the Spiro et al. model. Furthermore, the three models do not produce regions of maximum heating in the same locations, i.e., the maximum heating is found in the morning sector for the observed case and in the afternoon sector for the two statistical cases. The underestimation of the maximum Joule heating rate in the morning sector for the statistical cases can be attributed to the unrealistically high conductance value along the poleward portion of the westward electrojet, where the electric field is supposed to be more important than the conductance en-

36

hancement. All in all, these findings reassert the limitations of the presently available conductance models in simulating a 'realistic' situation in detail.

VIII. SUMMARY AND DISCUSSION

We have calculated various ionospheric electrodynamic parameters for the period of July 23-24, 1983, using ground magnetic records from a total of 88 stations in the northern hemisphere. For the first time, our results are based on an 'instantaneous' and 'realistic' conductance distribution deduced from DMSP-F6 bremsstrahlung X-ray image data. In this sense, the results are expected to clarify aome of the long-standing uncertainties about the outputs of magnetogram-inversion techniques combined with statistically derived conductance models. In particular, the electric potential distribution and the Joule heating rate have been reported to be considerably affected by the choice of the conductance models. Although our instantaneous conductance distributions deduced from the X-ray image data are the most realistic ones available at the present time, several limitations inherent in the instrument on board the DMSP-F6 spacecraft make some aspects of our results uncertain.

Due to its low-altitude orbit and the tilt of the geomagnetic axis from the rotational axis, the satellite field of view is limited, often leaving a significant portion of the nightside or dayside aurora out of the field of view. Thus, the unimaged areas have to be filled in using statistical methods. With respect to temporal limitations, the DMSP X-ray spectrometer takes approximately 17 minutes to scan the entire polar region, imposing a limit on the time resolution of the conductance distribution and making it difficult to investigate transient phenomena, such as the westward traveling surge, during the expansion phase of substorms. Perhaps the most serious problem relates to the satellite's orbital period. Since the satellite orbits the earth every 101 minutes, only one image is available during the period, or two images, if one uses the image taken over the other hemisphere. Having images so widely separated in time present a particularly serious limitation when one is investigating the sequential development of an individual substorm lasting for several hours. With such limitations in mind, we summarize here some important aspects of high-

latitude electrodynamics, in particular, those associated with substorms, focusing particularly on the features that have not been clear in studies based on statistical conductance models.

1. One of the most important findings of the present study is confirmation that the poleward portion of the westward electrojet in the morning sector is dominated by the electric field, while the equatorward portion is dominated by the conductance enhancement. Although it is less definite, a reverse trend seems to exist in the eastward electrojet in the dusk sector; the electric field dominates the equatorward portion, and the conductance enhancement dominates the poleward portion. On the other hand, however, the westward electrojet in the midnight sector, particularly during the maximum phase, seems to be dominated as a whole by the conductance enhancement. Such a finding would be unexpected from a statistically derived conductance model, which utilizes ground magnetic data directly or indirectly in the form of geomagnetic indices.

2. During quiet or moderately disturbed periods, in terms of the AE indices, the major electric potential structures are, in general, confined within the poleward region of the enhanced conductance belt. As mentioned just above, the westward electrojet in the midnight-morning sector straddles the two boundaries. As the magnetic activity increases, the electric potential pattern expands equatorward and becomes enhanced, as does the enhanced conductance region, thus maintaining the nearly identical spatial relationship between the electric field and the conductance enhancements in the postmidnight sector. However, the equatorward expansion of the electric potential pattern seems to exceed that of the enhanced conductance region. Furthermore, the poleward expansion of the conductance-enhanced zone leaves a significant portion of the electric potential structure embedded in the enhanced conductance region. This indicates that the electric field in the region seems to be somewhat short-circuited and as a consequence the cross-polar-cap potential difference is reduced. Since the conductance enhancement seems to compensate enough for the reduction in the electric field strength in the westward electrojet region, the magnetic activity in terms of the AE indices is expected to increase. It is interesting to recall that Reiff et al. (1981) reported that the cross-polar cap potential difference is less correlated with the AE index than with interplanetary parameters, such as the interplanetary electric field, $-\underline{V} \times \underline{B}$. One plausible explanation emerging from this study is that during the early phase of a substorm the electric field enhancement is apparently more important than the conductance enhancement, while the conductance enhancement seems to overshadow the electric field enhancement during the expansion phase

and thereafter. From the analysis of CDAW6 events, Kamide and Baumjohann (1985) have arrived at a similar conclusion.

3. There is a resemblance between the equivalent current system and the electric potential distribution as far as their global pattern is concerned. It is partly understandable, since the period examined in this study was during the summer season; so the ionospheric conductance distribution over a significant portion of the polar ionosphere was controlled by the solar UV radiation and changed slowly. On the other hand, in the nightside auroral region the major electric potential structures are found generally poleward of the enhanced conductance belt, where the conductance is low but relatively uniform. This seems to be another reason for the similarity. Significant discrepancies are noticed along the equatorward boundary of the westward electrojet in the postmidnight quadrant, where the conductance is more important than the electric field. However, such a small region is perhaps too insignificant to influence the overall potential pattern. There seems to be no reason to suppose that such a similarity is absent during the winter season. During the expansion phase of substorms and thereafter, which accompanies a strong conductance enhancement at the auroral region, however, more discrepancies between the equivalent current and potential patterns are expected within and near the region.

4. The electric potential distributions during the disturbed periods consist of, in general, a well-defined two-cell convection pattern. The whole pattern expands equatorward and becomes enhanced, as magnetic activity increases. It is interesting to mention that there are seldom any of the significantly localized structures that frequently appeared with the statistically derived conductance models. Thus, such features seem to be artifacts of the unrealistic conductance distribution. In particular, significant parts of the strongly enhanced potential structure frequently appearing in the subauroral zone, once believed to be the result of the assumed unrealistic vertical magnetic field line in the region (Kamide and Baumjohann, 1985), may in fact have something to do with the unrealistically low conductance value in the region. In other words, ionospheric current flow in the subauroral region seems to be dominated by the ionospheric conductance enhancement. The IMF B_y signatures of the electric potential pattern (mostly identified from the statistical studies) are clearly seen on an individual basis, too. However, the multicell nature of the convection pattern over the polar cap region during northward IMF periods is not clear in our results. During a strongly northward IMF period, a sunward convection flow was identified over the polar cap region. It is still not clear whether it is a portion of the multicell pattern or the distorted two-cell pattern suggested by Heppner and Maynard (1987).

5. During strongly northward IMF periods, significant activity in terms of ionospheric currents, field-aligned currents, and joule dissipation were registered in the polar cap. The globally integrated joule heating rate during these periods, mostly confined within the high-latitude polar region from the pole to approximately 75° in latitude, was as much as 1×10^{11} watts. As suggested by Meng and Makita (1987), the magnetosphere seems to be far from its ground state. Even during such periods, however, there is a weak but relatively well-defined conductance-enhanced zone along the night-side auroral latitude, suggesting that the auroral particle precipitation is a permanent feature in the polar ionosphere and occurs independently and/or out of phase with the electric field enhancement, as far as the northward IMF period is concerned.

6. The regions of intense joule heating are generally confined within relatively narrow belts along the auroral electrojets. In the morning sector, however, the strong heating region is shifted slightly poleward of the center of the westward electrojet, as a result of the relative importance of the electric field along its poleward boundary. Although not as prominent as in the westward electrojet region, there seems to be a reverse trend in the eastward electrojet region; the strong joule heating region tends to be located in its equatorward portion. As reported in earlier studies (Banks, 1977; Kamide and Baumjohann, 1985) however, the joule dissipation rate is found to be low in the local midnight sector, indicating that the conductance enhancement in the region is largely responsible for the current intensification, making the joule dissipation there insignificant. On the other hand, in spite of a relatively enhanced conductance distribution caused by the solar UV radiation, significant joule heating is found in the dayside cusp region. The situation in the polar cap region is somewhat different. During a disturbed period no significant heating occurs, but it turns out to be the most intense heating region during strongly northward IMF periods. This suggests that the physics governing the polar cap region during strongly northward IMF periods may be completely different from the physics of a disturbed period.

7. With some fine structures, the field-aligned current distribution patterns on an individual basis also show characteristics similar to those deduced from the statistical study of satellite data by Iijima and Potemra (1976). As reported in recent studies (Akasofu et al., 1980; Potemra et al., 1987), a systematic current pattern is identified poleward of the Region 1 current system, flowing upward in the morning sector and downward in the evening sector. It may be the Region 0 current system proposed by Heikkila (1984). It is interesting to note that the Region 2

upward current in the morning sector is roughly collocated with the enhanced conductance region, while this is not the case for the Region 1 upward current in the evening sector, indicating that the electron spectrum in the morning hemisphere is hard enough to produce a significant conductance enhancement. There is also a relatively strong field-aligned current distribution in the dayside cusp region without any accompanying conductance enhancement.

8. In spite of significant differences in the distribution patterns between the statistically derived conductance model and the 'instantaneous' case, the various ionospheric parameters based on the statistical models show remarkable similarities to those based on the X-ray image-based conductance distribution. Even the distribution patterns of the electric potential and the Joule heating rate, which were reported to be highly sensitive to the choice of conductance models, also show marked similarities. Thus, the statistical models can be used as a good first approximation for the study of polar ionospheric electrodynamics, as far as the global features are concerned. As shown earlier, however, for those who are interested in the spatial and temporal variations of the polar ionosphere, the inadequacy of the statistical model in simulating a 'realistic' conductance distribution is a serious limitation. There are several remaining problems that must be overcome before the presently available conductance model is capable of handling such subtle phenomena. Most of the empirical models assume a smooth, well-defined enhanced conductance zone along the auroral belt, with a predetermined location and intensity both parameterized by one of the geomagnetic indices. However, since there could be numerous possible configurations of the auroral electrojets, given the same level of magnetic activity in terms of the geomagnetic indices, such a predetermined belt is far from adequate for the highly dynamic situation, e.g., during the expansion phase of a substorm. One can correct such a limitation by shifting the enhanced conductance belt so as to match the enhanced current region (Kamide and Baumjohann, 1985). Quite often, however, this makes matters worse, by introducing a wrong shift of the belt with respect to the electrojet in other local time sectors. Furthermore, as shown in this study, there is no guarantee that the enhanced conductance zones always coincide with the enhanced current regions. On the other hand, there seems to be a tendency for the electric field enhancement to dominate the conductance enhancement in the early phase of a substorm and for the conductance enhancement to dominate in the expansion and following phases. If that is the case, the statistical models parameterized by ground magnetic data directly or indirectly, which are a manifestation of both electric field and conductance, would be unsuitable for studying the temporal development of substorms.

REFERENCES

Ahn, B.-H., E. Friis-Christensen, D.J. Gorney, Y. Kamide, H.W. Kroehl, P.F. Mizera, A.D. Richmond, C.G. Sucksdorf, and C.D. Wells, Numerical Modeling of Polar Ionospheric Electrodynamics for July 23-24, 1983 Utilizing Ionospheric Conductances Deduced from DMSP X-ray Images, WDC-A Report UAG-97, Boulder, CO., 1987.

Ahn, B.-H., Y. Kamide, and S.-I. Akasofu, "Global Ionospheric Current Distribution During Substorms," J. Geophys. Res., 89. 1613, 1984.

Ahn, B.-H., Y. Kamide, and S.-I. Akasofu, "Electrical Changes of the Polar Ionosphere During Magnetospheric Substorms," J. Geophys. Res., 91, 5737, 1986.

Ahn, B.-H., Y. Kamide, S.-I. Akasofu, and C.-I. Meng, "Convection Patterns in the Polar Ionosphere for Northward IMF Inferred from Ground-Based Magnetometer Data," J. Geomag. Geoelectr., 39, 313, 1987.

Ahn, B.-H., R.M. Robinson, Y. Kamide, and S.-I. Akasofu, "Electric Conductivities, Electric Fields and Auroral Particle Energy Injection Rate in the Auroral Ionosphere and Their Empirical Relations to the Horizontal Magnetic Disturbances, Planet. Space Sci., 31, 641, 1983.

Akasofu, S.-I., Physics of Magnetospheric Substorms, P. 81, D. Reidel, Hingham, Mass., 1977.

Akasofu, S.-I., "Evolution of Ideas in Solar-Terrestrial Physics," Geophys. J. R. Astr. Soc., 74, 257, 1983.

Akasofu, S.-I., J. Kisabeth, G.J. Romick, H.W. Kroehl, and B.-H. Ahn, "Day-to-Day Average Magnetic Variations Along the IMS Alaska Meridian Chain of Observatories and Modeling of a Three-Dimensional Current System," J. Geophys. Res., 85, 2005, 1980.

Banks, P.M., "Observations of Joule and Particle Heating in the Auroral Zone," J. Atmos. Terr. Phys., 39, 179, 1977.

Burke, W.J., M.C. Kelley, R.C. Sagalyn, M. Smiddy, and S.T. Lai, "Polar Cap Electric Field Structure with Northward IMF," Geophys. Res. Lett., 6, 21, 1979.

Bythrow, P.F., T.A. Potemra, L.J. Zanetti, R.A. Erlandson, D.A. Hardy, F.J. Rich and M.H. Acuna, "High Latitude Currents in the 0600 to 0900 MLT Sector: Observations from Viking and DMSP-F7," Geophys. Res. Lett., 14, 423, 1987.

Fayermark, E.S., "Reconstruction of the Three-Dimensional Current System of the High-Latitude Region from Ground-Based Geomagnetic Measurements," Geomagn. Aeron., Engl. Transl., 17, 114, 1977.

Foster, J.C., "Reply to Kamide and Richmond," Geophys. Res. Lett., 14, 160, 1987.

Friis-Christensen, E., Y. Kamide, A.D. Richmond, and S. Matsushita, "Interplanetary Magnetic Control of High-Latitude Electric Fields and Currents Deter ined from Greenland Magnetometer Data," J. Geophys. Res., 90, 1325, 1985.

Friis-Christensen, E., and J. Wilhjelm, "Polar Cap Currents for Different Directions of the Interplanetary Magnetic Field in the Y-Z Plane," J. Geophys. Res., 80, 1248, 1975.

Fuller-Rowell, T.J., and D.S. Evans, "Height Integrated Pedersen and Hall Conductivity Patterns Inferred from the TIROS-NOAA Satellite Data," J Geophys. Res., 92, 7606, 1987.

Gorney, D.J., P.F. Mizera and J.L. Roeder, A Maximum-Entropy Technique for Deconvolution of Atmospheric Bremsstrahlung Spectra, Space Sciences Laboratory Report No. SSL-86(6940-06)-06, The Aerospace Corporation, Los Angeles, CA, 1985.

Gustafsson, G., A Revised Corrected Geomagnetic Coordinate System, Kiruna Geophysical Observatory, Report No. 694, Royal Swedish Academy of Science, 1969.

Hardy, D.A., M.S. Gussenhoven, R. Raistrick, and W.J. McNeil, "Statistical and Functional Representations of the Pattern of Auroral Energy Flux, Number Flux and Conductivity," J. Geophys. Res., 92, 12275, 1987.

Heelis, R.A., P,H. Reiff, J.D. Winningham, and W.B. Hanson, "Ionospheric Convection Signatures Observed by DE-2 During Northward Interplanetary Magnetic Field," J. Geophys. Res., 91, 5817, 1986.

Heikkila, W.J., "Magnetospheric Topology of Fields and Currents," in Magnetospheric Currents, edited by T.A. Potemra, P. 208-222, American Geophysical Union, Washington, D.C., 1984.

Heppner, J.P., and N.C. Maynard, "Empirical High-Latitude Electric Field Models," J. Geophys. Res., 92, 4467, 1987.

Horwitz, J.L., and S.-I. Akasofu, "On the Relationship of the Polar Cap Current System to the North-South Component of the Interplanetary Magnetic Field," J. Geophys. Res., 84, 2507, 1979.

Iijima, T., and T.A. Potemra, "The Amplitude Distribution of Field-Aligned Currents at Northern High Latitudes Observed by Triad," J. Geophys. Res., 81, 2165, 1976.

Iijima, T., T.A. Potemra, L.J. Zanetti, and P.F. Bythrow, "Large-Scale Birkeland Currents in the Dayside Polar Region During Strongly Northward IMF: A New Birkeland Current System," J. Geophys. Res., 89, 7441, 1984.

Imhof, W.L., G.H. Nakano, R.G. Johnson, and J.B. Reagan, "Satellite Observations of Bremsstrahlung from Widespread Energetic Electron Precipitation Events," J. Geophys. Res., 79, 565, 1974.

Imhof, W.L., H.D. Voss, D.W. Datlowe, and J. Mobilia, "Bremsstrahlung X-Ray Images of Isolated Electron Patches at High Latitude," J. Geophys. Res., 90, 6515, 1985.

Imhof, W.L., H.D. Voss, D.W. Datlowe, and J. Mobilia, "Isolated Electron Precipitation Regions at High Latitudes," J. Geophys. Res., 93, 2649, 1988.

Kamide, Y., "The Two-Component Auroral Electrojet," Geophys. Res. Lett., 9, 1175, 1982.

Kamide, Y., B.-H. Ahn, S.-I. Akasofu, W. Baumjohann, E. Friis-Christensen, H.W. Kroehl, E. Maurer, A.D. Richmond, G. Rostoker, J. Walker, and A.N. Zaitzev, "Global Distribution of Ionospheric and Field-Aligned Currents During Substorms as Determined from Six IMS Meridian Chains of Magnetometers: Initial Results," J. Geophys. Res., 87, 8228, 1982.

Kamide, Y., and W. Baumjohann, "Estimation of Electric Fields and Currents from International Magnetospheric Study Magnetometer Data for the CDAW-6 Intervals: Implications for Substorm Dynamics," J. Geophys. Res., 90, 1305, 1985.

Kamide, Y., J.D. Craven, L.A. Frank, B.-H. Ahn, and S.-I. Akasofu, "Modeling Substorm Current Systems Using Conductivity Distributions Inferred from DE Auroral Images," J. Geophys. Res., 91, 11235, 1986.

Kamide, Y., H.W. Kroehl, B.A. Hausman, R.L. McPherron, S.-I. Akasofu, A.D. Richmond, P.H. Reiff, and S. Matsushita, "Numerical Modeling of Ionospheric Parameters from Global IMS Magnetometer Data for the CDAW-6 Interval," WDC-A Report UAG-88, Boulder, CO., 1983.

Kamide, Y., and S. Matsushita, "Simulation Studies of Ionospheric Electric Fields and Currents in Relation to Field-Aligned Currents, 1. Quiet Periods," J. Geophys. Res., 84, 4083, 1979.

Kamide, Y., and A.D. Richmond, "Ionospheric Conductivity Dependence of Electric Fields and Currents Estimated from Ground Magnetic Observations," J. Geophys. Res., 87, 8331, 1982.

Kamide, Y., A.D. Richmond, and S. Matsushita, "Estimation of Ionospheric Electric Fields, Ionospheric Currents and Field-Aligned Currents from Ground Magnetic Record," J. Geophys. Res., 86, 801, 1981.

Kamide, Y., and J.F. Vickrey, "Relative Contribution of Ionospheric Conductivity and Electric Field to the Auroral Electrojets," J. Geophys. Res., 88, 7989, 1983.

Kisabeth, J.L., "On Calculating Magnetic and Vector Potential Fields Due to Large-Scale Magnetospheric Current Systems and Induced Currents in an Infinitely Conducting Earth," in Quantitative Modeling of Magnetospheric Processes, ed. by W.P. Olson, Amer. Geophys. Union, p. 473-498, 1979.

Kroehl, H.W., and A.D. Richmond, "Magnetic Substorm Characteristics Described by Magnetic Potential Map for 26-28 March 1976," in Dynamics of the Magnetosphere. ed. by S.-I. Akasofu, p. 269, D. Reidel, Hingham, Mass., 1980.

Levitin, A.E., R.G. Afonina, B.A. Belov, and Y.I. Feldstein, "Geomagnetic Variation and Field-Aligned Currents at Northern High-Latitudes, and Their Relations to the Solar Wind Parameters," Philos. Trans. R. Soc. London, Ser. A 304, 253, 1982.

Maezawa, K., "Magnetospheric Convection Induced by the Positive and Negative Z Components of the Interplanetary Magnetic Field; Quantitative Analysis Using Polar Cap Magnetic Records," J. Geophys. Res., 81, 2289, 1976.

Meng, C.-I., and K. Makita, "What is the Ground State of the Solar-Terrestrial Interaction? (abstract), Quantitative modeling of magnetosphere-ionosphere coupling processes, ed. by Y. Kamide and R.A. Wolf, p. 217, Kyoto, Japan, 1987.

Mishin, V.M., A.D. Bazarzhapov, and G.V. Shpynev, "Electric Fields and Currents in the Earth's Magnetosphere," in Dynamics of the Magnetosphere, ed. by S.-I. Akasofu, p. 249-268, D. Reidel, Hingham, Mass., 1980.

Mizera, P.F., D.J. Gorney, and D.S. Evans, "On the Conjugacy of the Aurora: High and Low Latitudes," Geophys. Res. Lett., 14, 190, 1987.

Mizera, P.F., D.J. Gorney, and J.L. Roeder, "Auroral X-Ray Images from DMSP-F6," Geophys. Res. Lett., 11, 255, 1984.

Mizera, P.F., W.A. Kolasinski, D.J. Gorney, and J.L. Roeder, "An Auroral X-Ray Imaging Spectrometer," J. Spacecraft and Rockets, 22, 514, 1985.

Mizera, P.F., J.G. Luhman, W.A. Kolasinski, and J.B. Blake, "Corrected Observations of Auroral Arcs, Electrons and X-Rays from a DMSP Satellite," J. Geophys. Res., 83, 5573, 1978.

Potemra, T.A., L.J. Zanetti, R.E. Erlandson, P.F. Bythrow, G. Gustafsson, M.H. Acuna, and R. Lundin, "Observations of Large-Scale Birkeland Currents with Viking," Geophys. Res. Lett., 14, 419, 1987.

Reiff, P.H., "Sunward Convection in Both Polar Caps," J. Geophys. Res., 87, 5976, 1982.

Reiff, P.H., R.W. Spiro, and T.W. Hill, "Dependence of Polar Cap Potential Drop on Interplanetary Parameters," J. Geophys. Res., 86, 7039, 1981.

Rezhenov, B.V., "Convection at High Latitude When the Interplanetary Magnetic Field is Northward," Planet. Space Sci., 29, 687, 1981.

Richmond, A.D., and Y. Kamide, "Mapping Electrodynamic Features of the High-Latitude Ionosphere from Localized Observations: Technique," J. Geophys. Res., submitted, 1987.

Robinson, R.M., F, Rich, and R.R. Vondrak, "Chatanika Radar and S3-2 Measurements of Auroral Zone Electrodynamics in the Midnight Sector," J. Geophys. Res., 90, 8487, 1985.

Robinson, R.M., R.R. Vondrak, K. Miller, T. Dabbs, and D. Hardy, "On Calculating Ionospheric Conductances from the Flux and Energy of Precipitating Electrons," J. Geophys. Res., 92, 2567, 1987.

Robinson, R.M., R.R. Vondrak, and T.A. Potemra, "Electrodynamic Properties of the Evening Sector Ionosphere Within the Region 2 Field-Aligned Current Sheet," J. Geophys. Res., 87, 731, 1982.

Rostoker, G., Y. Kamide, and J.D. Winningham, "Energetic Particle Precipitation into the High-Latitude Ionosphere and the Auroral Electrojets 3. Characteristics of Electron Precipitation into the Morning Sector Auroral Oval," J. Geophys. Res., 90, 7495, 1985.

Rostoker, G., and T.D. Phan, "Variation of Auroral Electrojet Spatial Location as a Function of the Level of Magnetospheric Activity," J. Geophys. Res., 91, 1716, 1986.

Rostoker, G., J.D. Winningham, K. Kawasaki, J.R. Burrows, and T.J. Hughes, "Energetic Particle Precipitation into the High-Latitude Ionosphere and the Auroral Electrojets 2. Eastward Electrojet and Field-Aligned Current Flow at the Dusk Meridian," J. Geophys. Res., 84, 2006, 1979.

Senior, C., R.M. Robinson, and T.A. Potemra, "Relationship Between Field-Aligned Currents, Diffuse Auroral Precipitation and the Westward Electrojet in the Early Morning Sector," J. Geophys. Res., 87, 10469, 1982.

Spiro, R.W., P.H. Reiff, and L.J. Maher, Jr., "Precipitating Electron Energy Flux and Auroral Zone Conductances: An Empirical Model," J. Geophys. Res., 87, 8215, 1982.

Strickland, D.J., J.R. Jasperse, and J.A. Whalen, "Dependence of Auroral FUV Emissions on the Incident Electron Spectrum and Neutral Atmosphere," J. Geophys. Res., 88, 8051, 1983.

Vickrey, J.F., R.R. Vondrak, and S.J. Matthews, "The Diurnal and Latitudinal Variation of Auroral Zone Ionospheric Conductivity," J. Geophys. Res., 86, 65, 1981.

Vickrey, J.F., R.R. Vondrak, and S.J. Matthews, "Energy Deposition by Precipitating Particles and Joule Dissipation in the Auroral Ionosphere," J. Geophys. Res., 87, 5184, 1982.

Vondrak, R.R., R.M. Robinson, P.F. Mizera, and D.J. Gorney, "X-Ray Spectro-Photometric Remote Sensing of Auroral Ionization," Radio Science. in press, 1988.

Wallis, D.D., and E.E. Budzinski, "Empirical Models of Height-Integrated Conductivities," J. Geophys. Res., 86, 125, 1981.

Zanetti, L.J., T.A. Potemra, T. Iijima, W. Baumjohann, and P.F. Bythrow, "Ionospheric and Birkeland Current Distributions for Northward Interplanetary Magnetic Field; Inferred Polar Convection," J. Geophys. Res., 89, 7453, 1984.

Table 1. Location of Magnetic Stations

	STATION NAME	CORRECTED GEOGRAPHIC		GEOMAGNETIC	
		LAT	LONG	LAT	LONG
1	Abisko	68.36	18.82	65.04	103.55
2	Alert	82.50	297.50	86.77	124.34
3	Alma Ata	43.25	76.92	37.97	148.71
4	Alta	68.86	22.96	66.23	107.61
5	Arkhangelsk	64.60	40.50	60.18	118.02
6	Baker Lake	64.33	263.97	75.15	319.99
7	Barrow	71.32	203.38	69.67	248.14
8	Bear Island	74.50	19.20	71.04	110.18
9	Borok	58.03	38.97	53.56	114.21
10	Boulder	40.14	254.76	49.50	315.70
11	Cambridge Bay	69.20	255.00	77.84	299.70
12	Cape Chelyuskin	77.72	104.28	71.58	174.19
13	Cape Parry	70.17	241.70	74.61	273.58
14	Cape Wellen	66.16	190.17	62.50	242.59
15	College	64.86	211.90	64.84	259.65
16	Daneborg	74.30	339.18	75.90	84.30
17	Danmarkshavn	76.80	341.40	77.60	91.70
18	Del Rio	29.49	259.08	38.70	325.00
19	Dixon Island	73.54	80.56	68.31	154.69
20	Fort Churchill	58.77	265.90	70.27	326.01
21	Fort Simpson	61.75	238.77	67.69	289.42
22	Fort Smith	60.00	248.00	68.20	299.30
23	Fort Yukon	66.57	214.73	66.98	260.10
24	Frederikshab	62.00	310.30	70.50	39.30
25	Furstenfeldbruck	48.17	11.28	45.00	87.61
26	Godthab	64.18	308.28	72.90	38.40
27	Godhavn	69.25	306.47	77.62	41.58
28	Great Whale River	55.27	282.22	67.96	353.76
29	Guam	13.58	144.87	6.90	213.70

30	Heiss Island	80.62	58.05	74.80	144.40
31	Honolulu	21.32	202.00	21.73	267.56
32	Inuvik	68.25	226.70	71.13	268.20
33	Kanoya	31.42	130.88	25.70	200.80
34	Karaganda	49.82	73.08	44.87	145.04
35	Kautokeino	69.02	23.05	65.42	107.03
36	Kazan	55.83	48.85	51.23	122.43
37	Kevo	69.80	27.00	66.30	110.60
38	Kilpisjarvi	69.05	207.00	65.56	105.28
39	Kiruna	67.83	20.42	64.80	104.20
40	Kuvdlorssuaq	74.57	302.82	81.80	47.57
41	Leirvogur	64.18	338.30	66.82	69.60
42	Leningrad	59.95	30.71	55.82	107.77
43	Lynn Lake	56.85	258.93	66.95	319.08
44	M'Bour	14.39	343.04	10.70	57.70
45	Magadan	60.12	151.02	53.90	217.40
46	Meanook	54.62	246.67	62.61	300.90
47	Memambetsu	43.91	144.19	37.40	213.70
48	Minsk	54.10	26.50	50.35	101.88
49	Moscow	55.48	37.31	50.97	112.01
50	Mould Bay	76.20	240.60	80.56	263.54
51	Muonionalusta	68.02	23.53	64.39	106.60
52	Narssarssuaq	61.10	314.60	68.90	44.00
53	New Aalesund	78.92	11.93	75.90	114.70
54	Niemegk	52.07	12.68	47.97	90.01
55	Nord	81.60	343.24	80.80	111.70
56	Norman Wells	64.90	234.50	69.69	282.02
57	Novosibirsk	55.03	82.90	50.07	155.02
58	Nurmijarvi	60.51	24.66	56.62	103.05
59	Odessa	46.78	30.88	42.30	103.66
60	Ottawa	45.40	284.45	58.50	356.21
61	Pello	68.53	270.48	63.25	106.25
62	P. Tunguska	61.60	90.00	56.50	162.46

63	Resolute Bay	74.70	265.10	84.14	304.33
64	Sachs Harbor	72.00	235.00	76.25	272.94
65	Saint Johns	47.60	307.32	57.60	29.12
66	San Juan	18.11	293.85	31.47	5.54
67	Scoresbysund	70.48	338.03	71.98	75.39
68	Sitka	57.06	224.68	59.82	277.77
69	Sodankyla	67.37	26.63	63.56	108.54
70	Sondre Strom	67.02	309.28	75.20	42.60
71	Soroya	70.54	22.22	66.97	107.74
72	Sverdlovsk	56.73	61.07	52.70	132.50
73	Talkeetna	63.30	209.90	61.90	259.80
74	Tashkent	41.33	69.62	37.19	139.62
75	Tbilisi	42.09	44.71	37.40	115.30
76	Thule	77.48	290.83	86.77	39.20
77	Tixie Bay	71.58	129.00	65.82	195.48
78	Toledo*	39.88	355.95	33.91	73.17
79	Tromso	69.66	18.95	66.75	104.78
80	Tucson	32.25	249.17	39.88	311.36
81	Umanak	70.70	307.80	78.60	46.00
82	Upernavik	72.80	303.80	81.00	44.80
83	Valentia	51.93	349.75	50.06	71.77
84	Victoria*	48.52	236.58	54.12	292.40
85	Wingst	53.74	9.07	50.08	87.67
86	Witteveen	52.81	6.67	49.21	85.42
87	Yakutsk	62.02	129.72	55.71	199.83
88	Yellowknife	62.40	245.50	69.94	294.38

* Used only for July 24, 1983
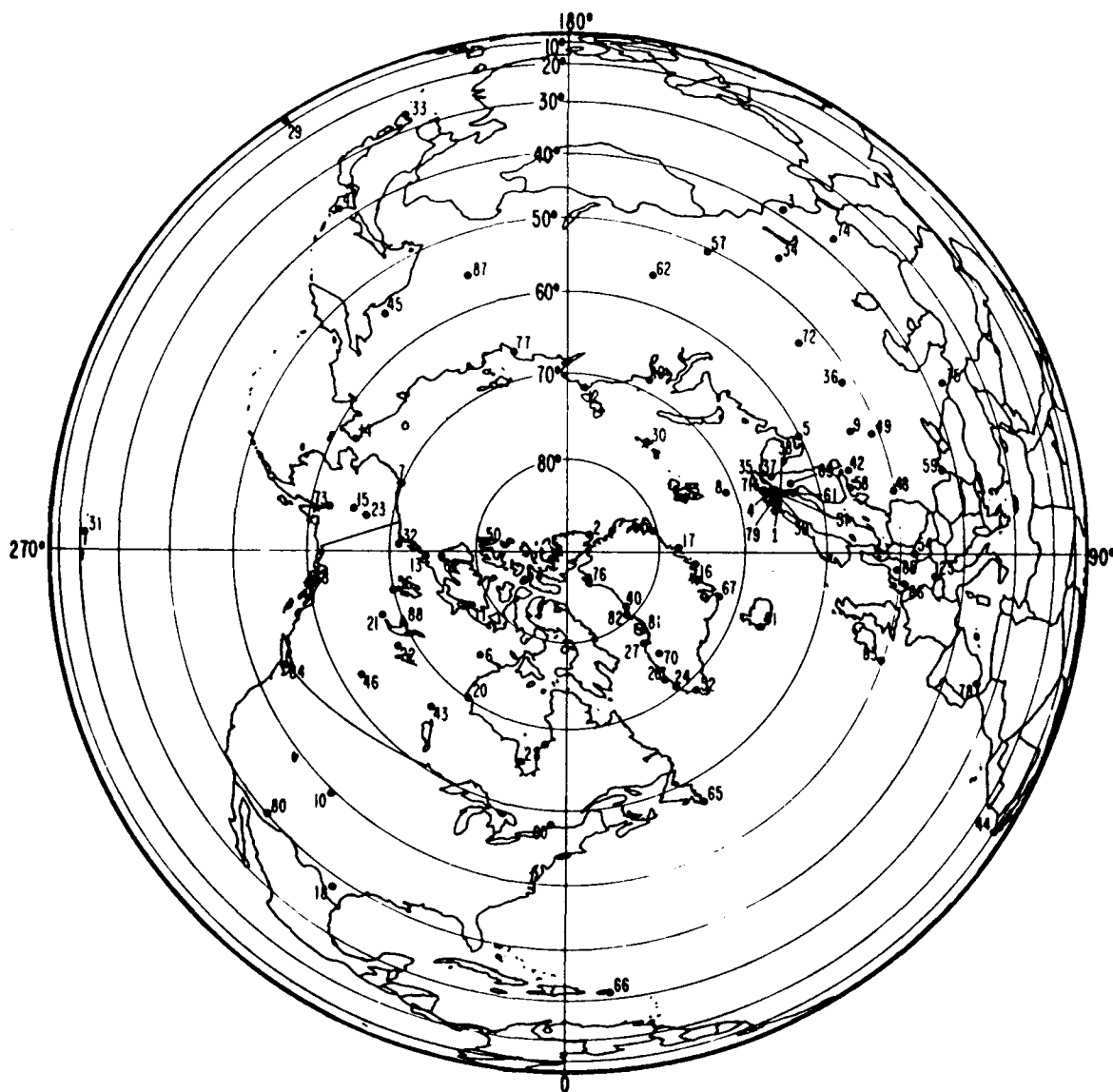
Fig. 1
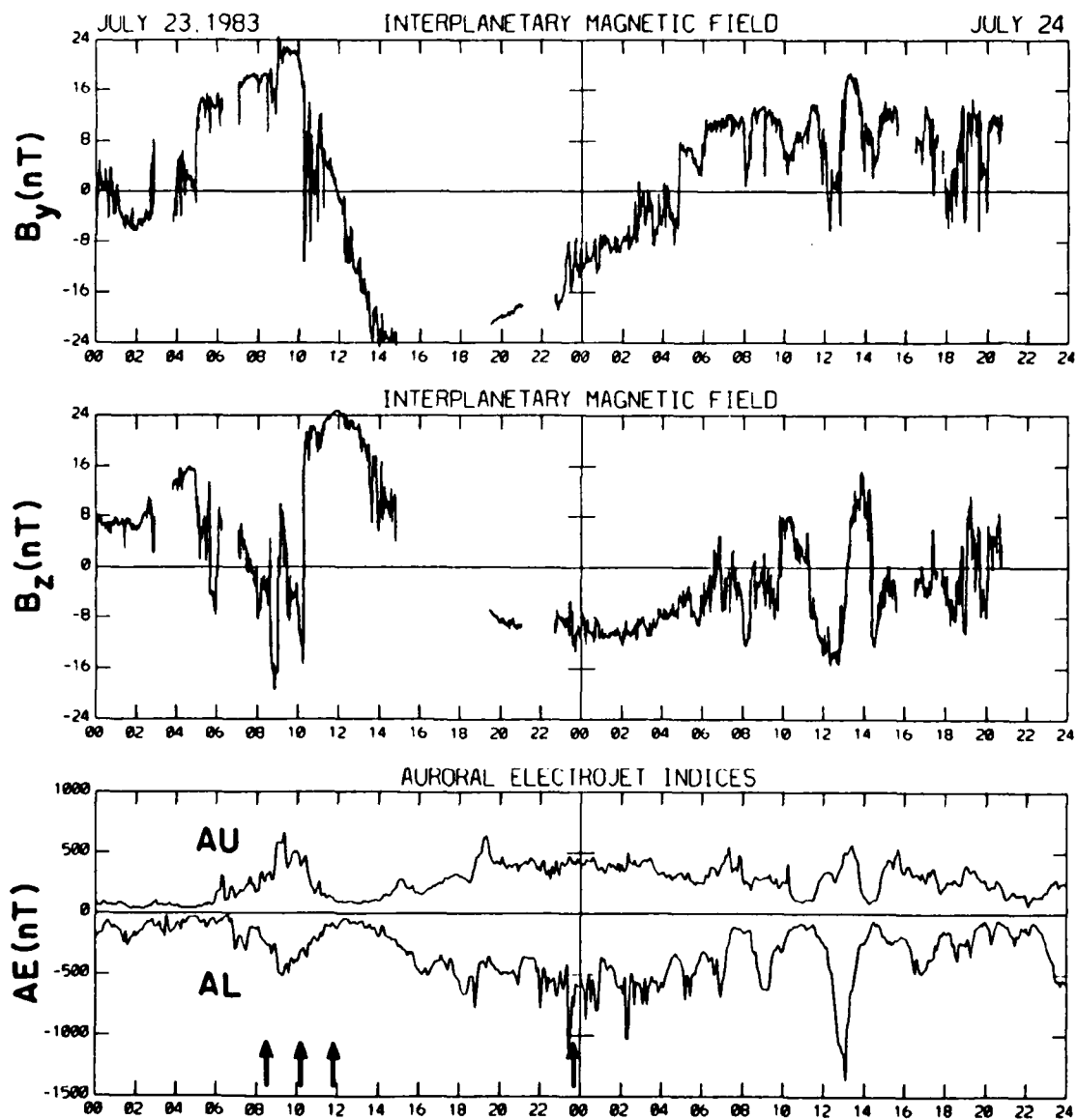
55

Fig. 2

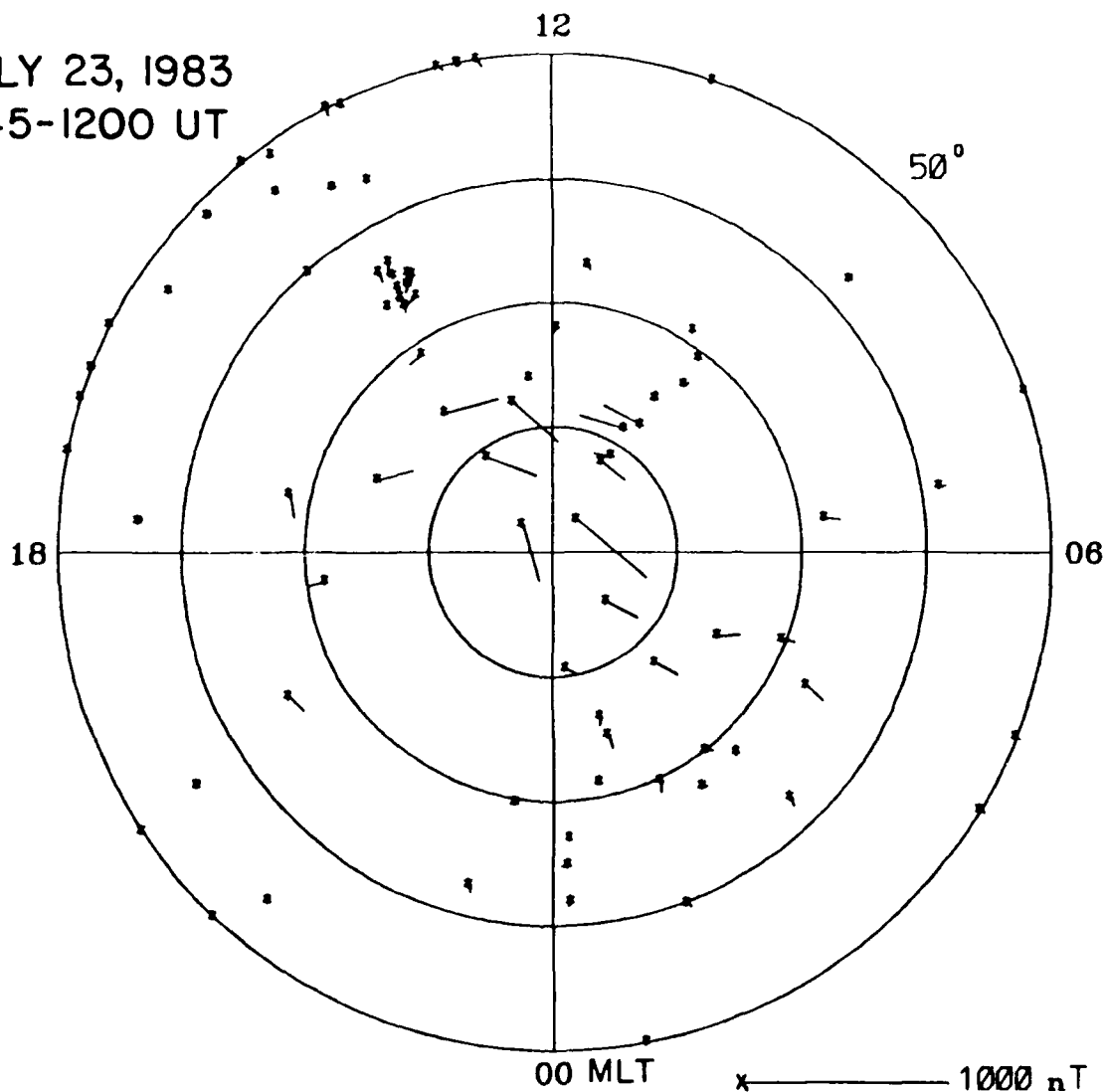56

EQUIVALENT CURRENT SYSTEM

JULY 23, 1983
825-840 UT
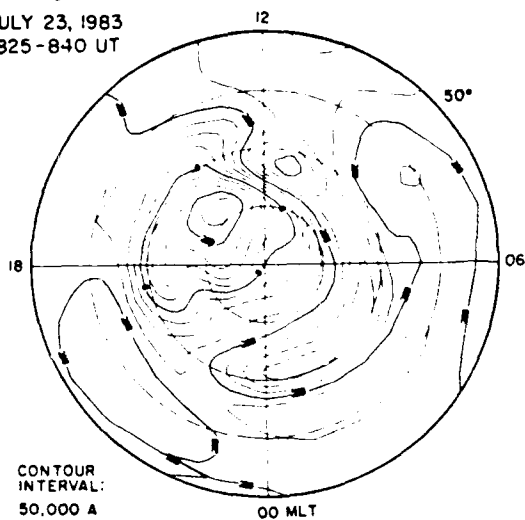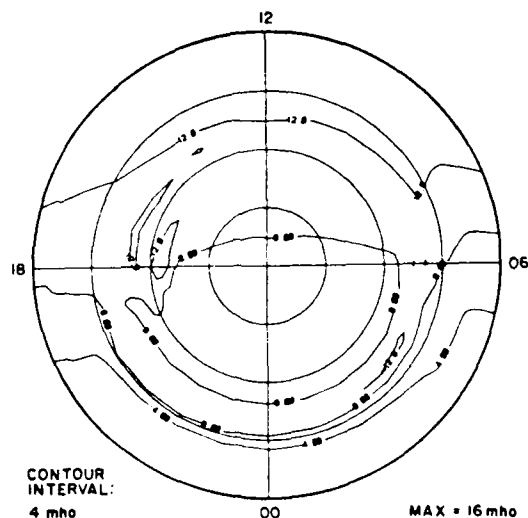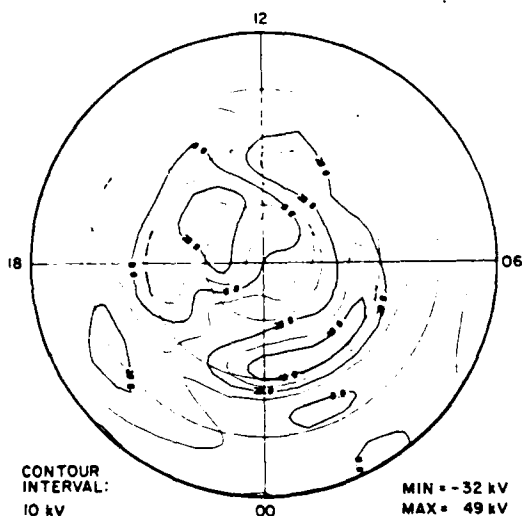
50°

18   06

CONTOUR
INTERVAL:
50,000 A   00 MLT

HALL CONDUCTANCE

18   06

CONTOUR
INTERVAL:
4 mho   00   MAX = 16 mho

ELECTRIC POTENTIAL

18   06

CONTOUR
INTERVAL:
10 kV   00   MIN = -32 kV
                    MAX = 49 kV

IONOSPHERIC CURRENT VECTORS

18   06

2 A/m

00

FIELD-ALIGNED CURRENTS

—— downward
----- upward

18   06

CONTOUR
INTERVAL:
0.3 μA/m²   00   MIN = -1.7 μA/m²
                      MAX = 2.2 μA/m²

JOULE HEATING RATE

18   06

CONTOUR
INTERVAL:
5 mW/m²

Watt
0.178E + 11
0.103E + 12
0.160E + 12   00   MAX = 59 mW/m²
0.165E + 12
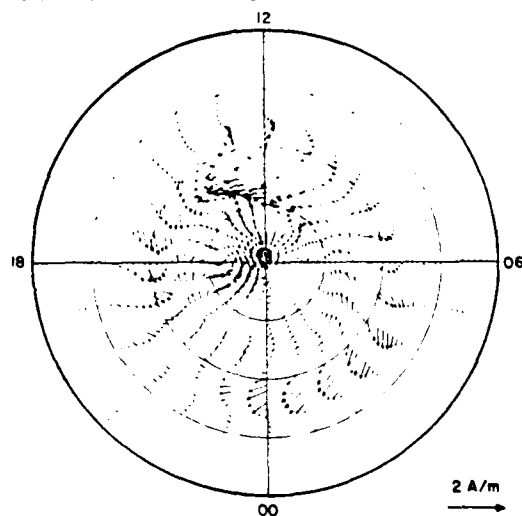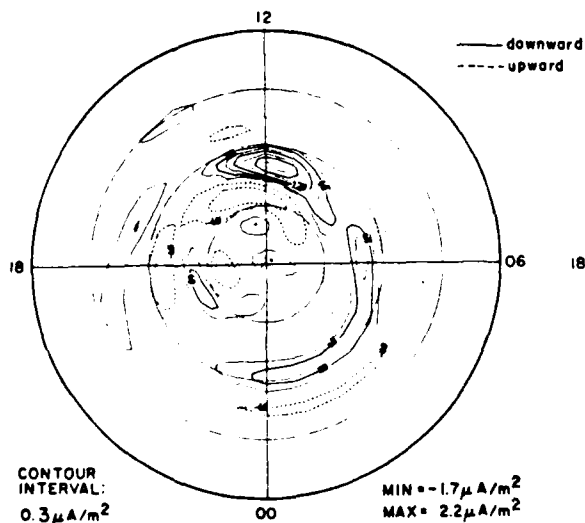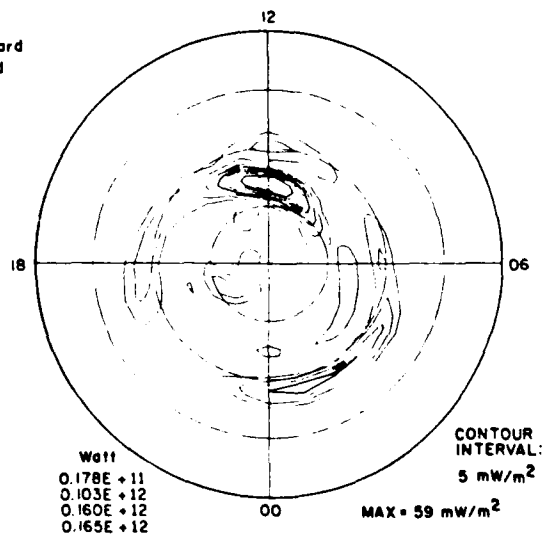
Fig. 3

ELECTRIC POTENTIAL AND HALL CONDUCTANCE

JULY 23, 1983
825-840 UT

JULY 23, 1983
2340-2355 UT

12

12

50°

18

06

18

06

CONTOUR
INTERVAL:
10 kV

00 MLT

MIN = -32 kV
MAX = 49 kV

00

MIN = -47 kV
MAX = 34 kV
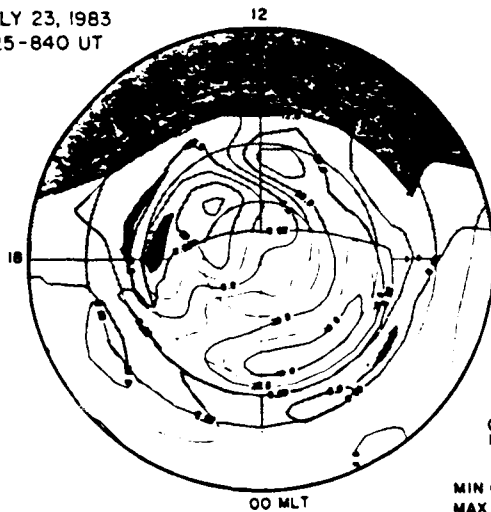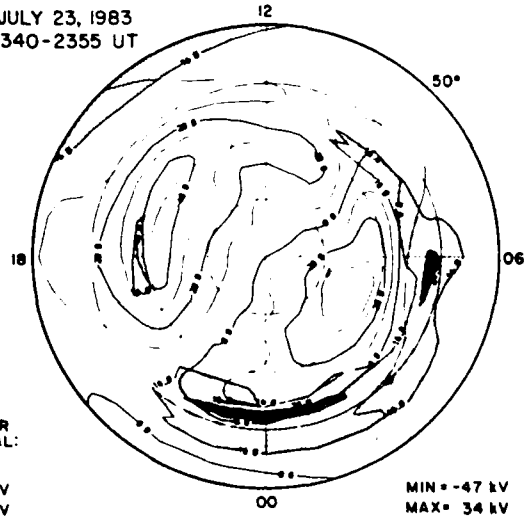
IONOSPHERIC CURRENT VECTORS AND HALL CONDUCTANCE

12

12

18

06

18

06

2 A/m

above 8 mho
4 ~ 8 mho

00

above 24 mho
16 ~ 24 mho

00

Fig. 4

58

EQUIVALENT CURRENT SYSTEM

JULY 23, 1983
1005-1020 UT

50°

12

18

06

CONTOUR
INTERVAL:
50,000 A

00 MLT

HALL CONDUCTANCE

12

18

06

00

CONTOUR
INTERVAL:
4 mho

MAX = 21 mho

ELECTRIC POTENTIAL

12

18

06

00

CONTOUR
INTERVAL:
10 kV

MIN = -59 kV
MAX = 50 kV

IONOSPHERIC CURRENT VECTORS

12

18

06

00

2 A/m

FIELD-ALIGNED CURRENTS

——— downward
----- upward

12

18

06

00

CONTOUR
INTERVAL:
0.3 μA/m²

MIN = -2.4 μA/m²
MAX = 2.6 μA/m²

JOULE HEATING RATE

12

18

06

00

Watt
0.307E + 11
0.177E + 12
0.274E + 12
0.278E + 12

CONTOUR
INTERVAL:
5 mW/m²

MAX = 69 mW/m²

Fig. 5

59

EQUIVALENT CURRENT VECTORS

JULY 23, 1983
1145-1200 UT
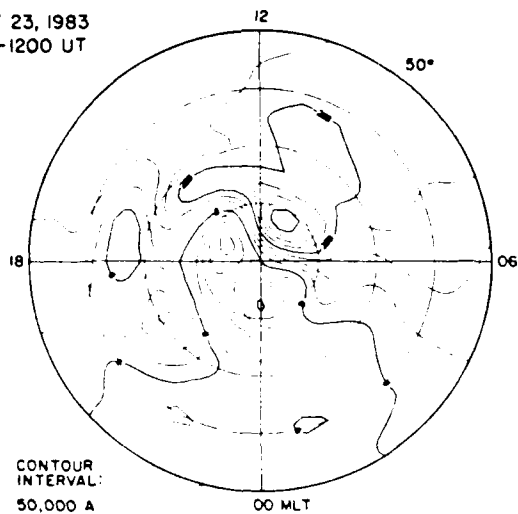
12

50°

18

06

00 MLT

x —————— 1000 nT

Fig. 6

60

EQUIVALENT CURRENT SYSTEM

JULY 23, 1983
1145-1200 UT

12

50°

18

06

CONTOUR
INTERVAL:

50,000 A

00 MLT

HALL CONDUCTANCE

12

18

06

CONTOUR
INTERVAL:

4 mho

00

MAX = 19 mho

ELECTRIC POTENTIAL

12

18

06

CONTOUR
INTERVAL:

10 kV

00

MIN = -46 kV
MAX = 20 kV

IONOSPHERIC CURRENT VECTORS

12

18

06

00

2 A/m

FIELD-ALIGNED CURRENTS

12

—— downward
----- upward

18

06

CONTOUR
INTERVAL:

0.3 μA/m²

00

MIN = -2.9 μA/m²
MAX = 2.0 μA/m²

JOULE HEATING RATE

12

18

06

Watt

0.579E + 11
0.104E + 12
0.117E + 12
0.119E + 12

00

CONTOUR
INTERVAL:

5 mW/m²

MAX = 61 mW/m²

Fig. 7

61

EQUIVALENT CURRENT SYSTEM

JULY 23, 1983
2340-2355 UT

12

50°

18   06

CONTOUR
INTERVAL:
50,000 A   00 MLT

HALL CONDUCTANCE

12

18   06

CONTOUR
INTERVAL:
4 mho   00   MAX = 26 mho

ELECTRIC POTENTIAL

12

18   06

CONTOUR
INTERVAL:
10 kV   00   MIN = -47 kV
          MAX = 34 kV

IONOSPHERIC CURRENT VECTORS

12

18   06

00   2 A/m

FIELD-ALIGNED CURRENTS

12

—— downward
----- upward

18   06

CONTOUR
INTERVAL:
0.3 μA/m²   00   MIN = -1.7 μA/m²
          MAX = 1.9 μA/m²

JOULE HEATING RATE

12

18   06

Watt
0.170E+11
0.693E+11   00
0.203E+12
0.216E+12
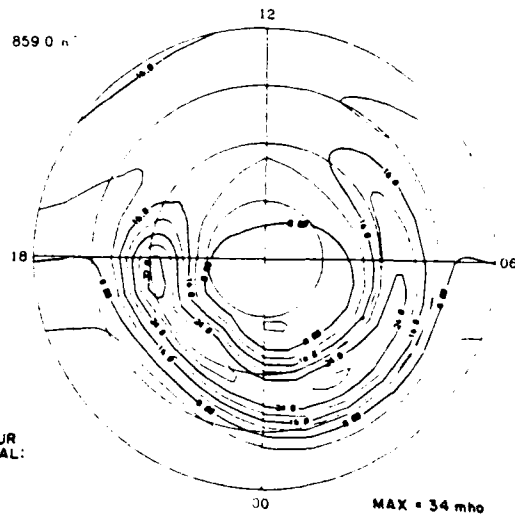
CONTOUR
INTERVAL:
5 mW/m²

MAX = 51 mW/m²

Fig. 8

62
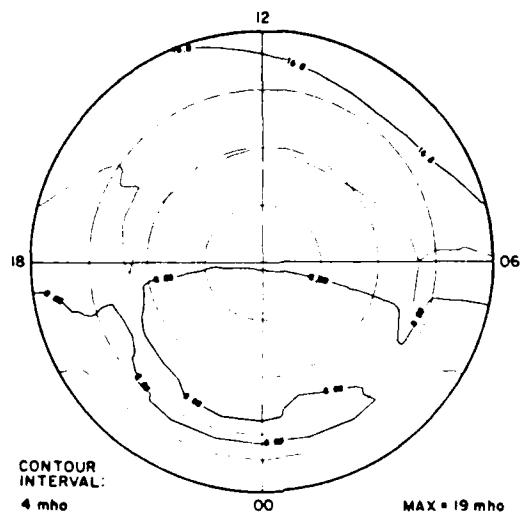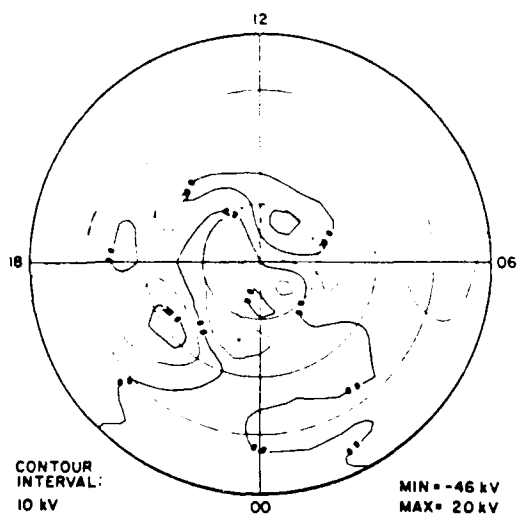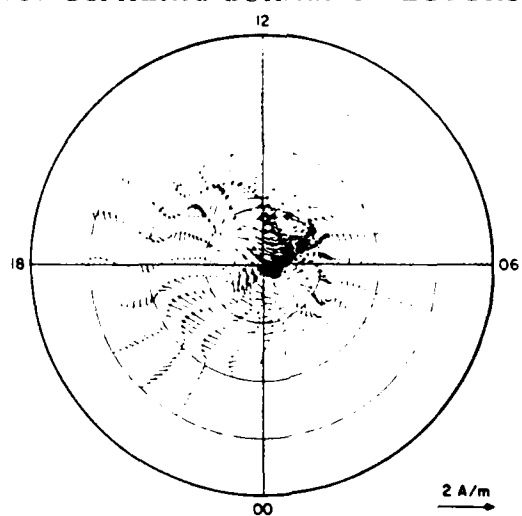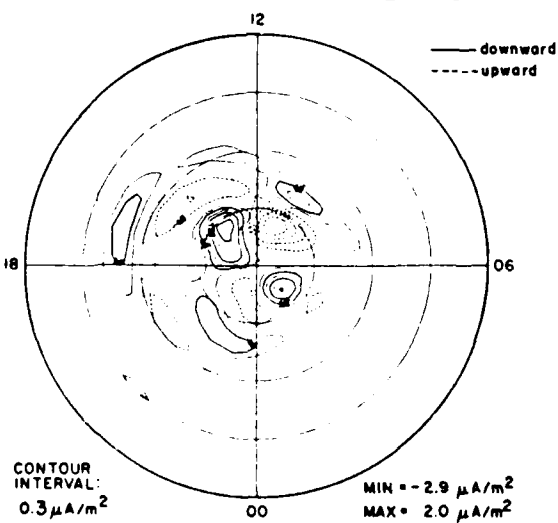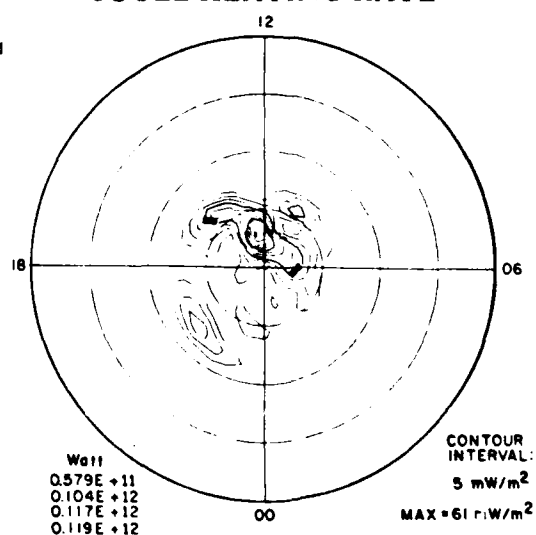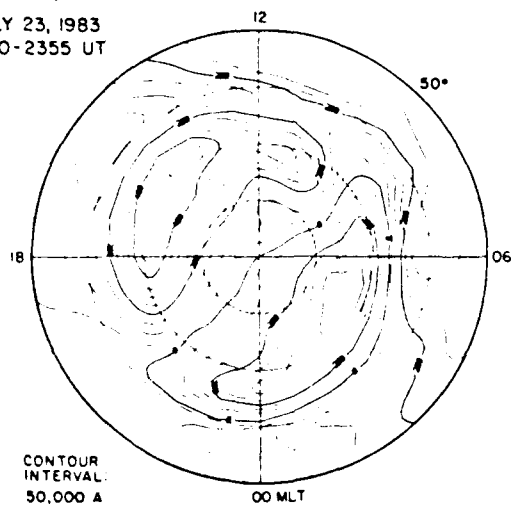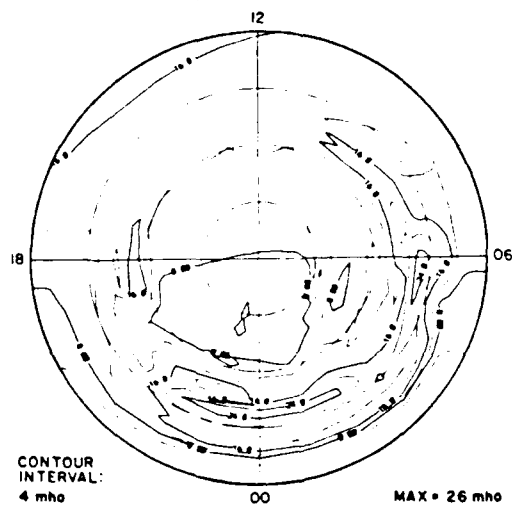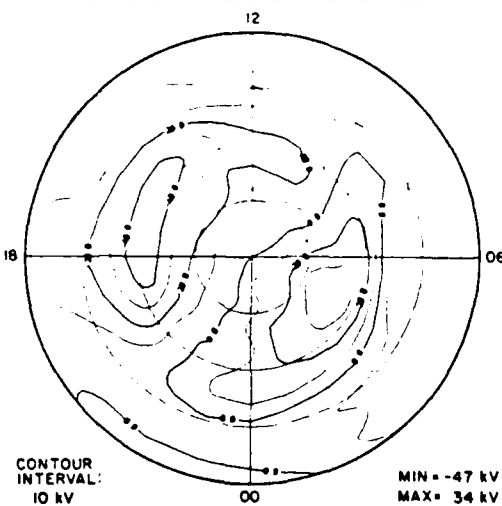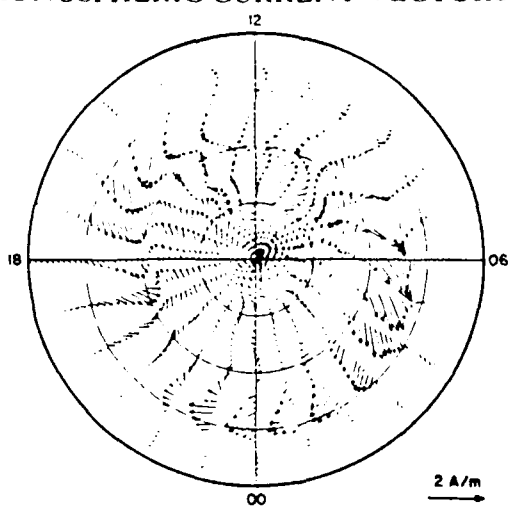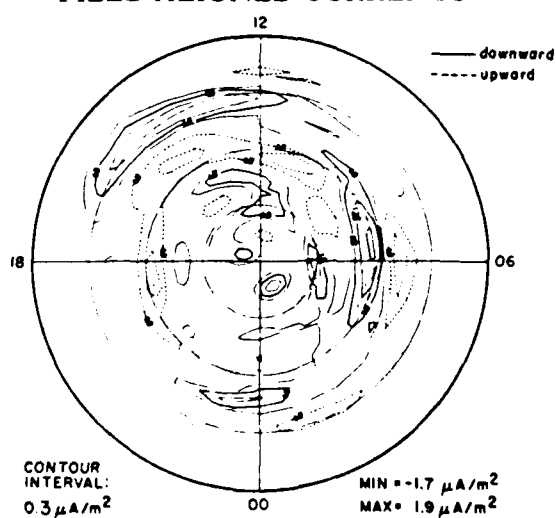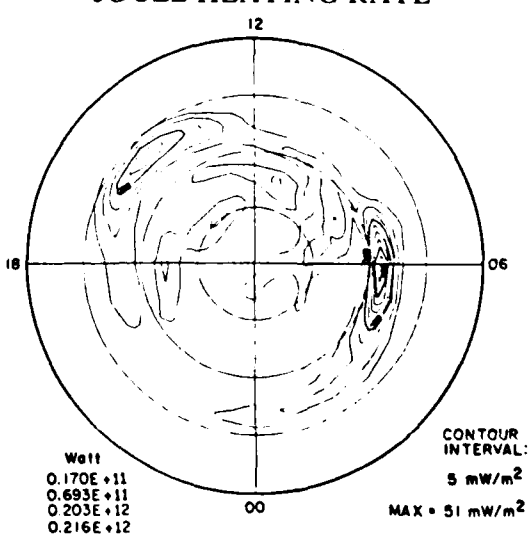
Ahn et al.(1983)   Spiro et al.(1982)

HALL CONDUCTANCE

JULY 23, 1983
2340-2355 UT
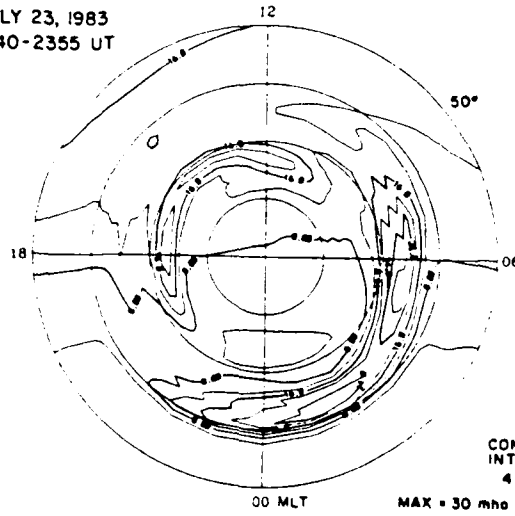
AE= 8590 n

CONTOUR
INTERVAL:
4 mho

MAX = 30 mho   MAX = 34 mho

ELECTRIC POTENTIAL

CONTOUR
INTERVAL:
10 kV

MIN = -45 kV   MIN = -34 kV
MAX = 40 kV   MAX = 34 kV

JOULE HEATING RATE

CONTOUR
INTERVAL:
5 mW/m²

Total
0.20E + 12 Watt

Total
0.19E + 12 Watt

MAX = 26 mW/m²   MAX = 30 mW/m²
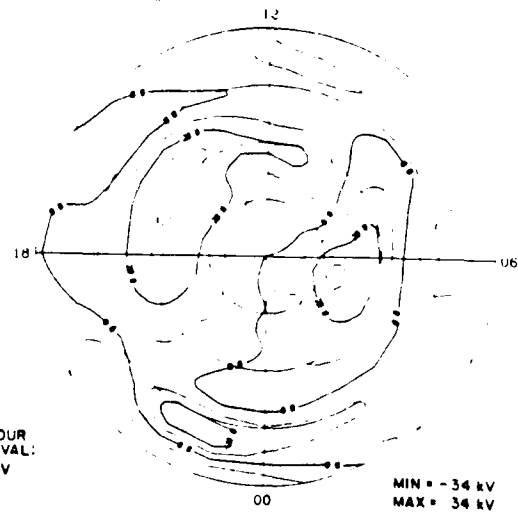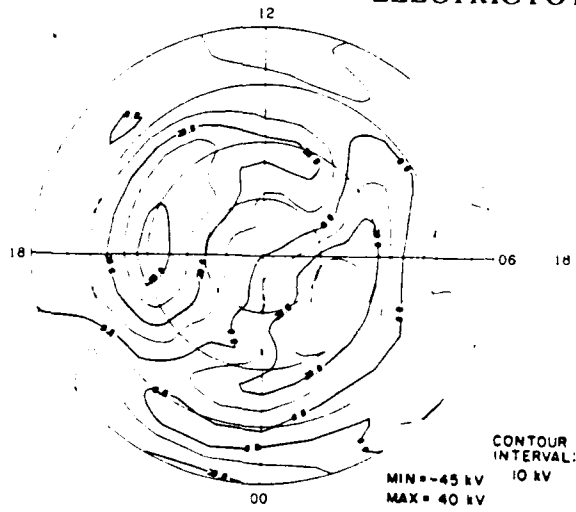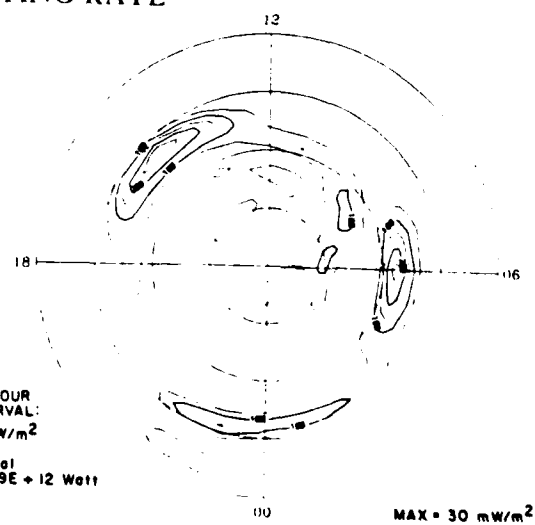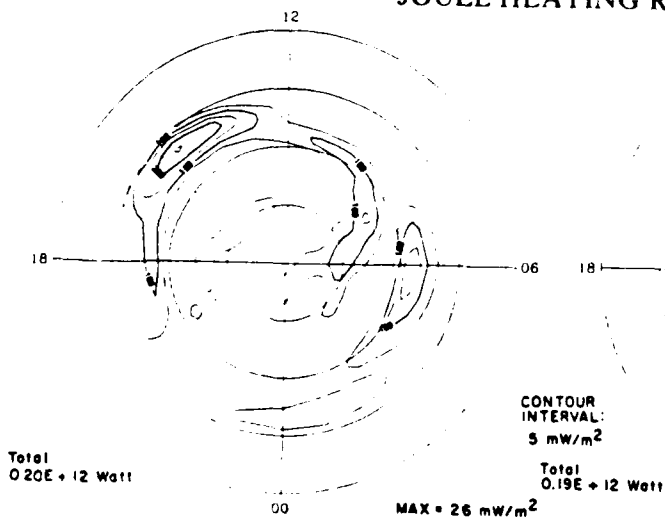
Fig. 9

The Aerospace Corporation functions as an "architect-engineer" for national security projects, specializing in advanced military space systems. Providing research support, the corporation's Laboratory Operations conducts experimental and theoretical investigations that focus on the application of scientific and technical advances to such systems. Vital to the success of these investigations is the technical staff's wide-ranging expertise and its ability to stay current with new developments. This expertise is enhanced by a rese.rch program aimed at dealing with the many problems associated with rapidly evolving space systems. Contributing their capabilities to the research effort are these individual laboratories:

Aerophysics Laboratory: Launch vehicle and reentry fluid mechanics, heat transfer and flight dynamics; chemical and electric propulsion, propellant chemistry, chemical dynamics, environmental chemistry, trace detection; spacecraft structural mechanics, contamination, thermal and structural control; high temperature thermomechanics, gas kinetics and radiation; cw and pulsed chemical and excimer laser development including chemical kinetics, spectroscopy, optical resonators, beam control, atmospheric propagation, laser effects and countermeasures.

Chemistry and Physics Laboratory: Atmospheric chemical reactions, atmospheric optics, light scattering, state-specific chemical reactions and radiative signatures of missile plumes, sensor out-of-field-of-view rejection, applied laser spectroscopy, laser chemistry, laser optoelectronics, solar cell physics, battery electrochemistry, space vacuum and radiation effects on materials, lubrication and surface phenomena, thermionic emission, photosensitive materials and detectors, atomic frequency standards, and environmental chemistry.

Computer Science Laboratory: Program verification, program translation, performance-sensitive system design, distributed architectures for spaceborne computers, fault-tolerant computer systems, artificial intelligence, microelectronics applications, communication protocols, and computer security.

Electronics Research Laboratory: Microelectronics, solid-state device physics, compound semiconductors, radiation hardening; electro-optics, quantum electronics, solid-state lasers, optical propagation and communications; microwave semiconductor devices, microwave/millimeter wave measurements, diagnostics and radiometry, microwave/millimeter wave thermionic devices; atomic time and frequency standards; antennas, rf systems, electromagnetic propagation phenomena, space communication systems.

Materials Sciences Laboratory: Development of new materials: metals, alloys, ceramics, polymers and their composites, and new forms of carbon; non-destructive evaluation, component failure analysis and reliability; fracture mechanics and stress corrosion; analysis and evaluation of materials at cryogenic and elevated temperatures as well as in space and enemy-induced environments.

Space Sciences Laboratory: Magnetospheric, auroral and cosmic ray physics, wave-particle interactions, magnetospheric plasma waves; atmospheric and ionospheric physics, density and composition of the upper atmosphere, remote sensing using atmospheric radiation; solar physics, infrared astronomy, infrared signature analysis; effects of solar activity, magnetic storms and nuclear explosions on the earth's atmosphere, ionosphere and magnetosphere; effects of electromagnetic and particulate radiations on space systems; space instrumentation.

. . .